The Meso-NH Atmospheric Simulation System:

Scientific Documentation

Part II: Model Setup

Acknowledgments

This volume contains contributions from P. Bechtold, S. Belair, Ph. Bougeault, J.M. Carrière, J. Cuxart, V. Ducrocq, C. Fischer, M. Georgelin, P. Héreil, J.-P. Lafore, C. Liousse, C. Mari, I. Mallet, P. J. Mascart, V. Masson, J.-P. Pinty, E. Richard, K. Suhre, J. Stein, P. Tulet, and J. Vilà-Guerau de Arellano. As editors, we would like to express our deep appreciation for the dedicated work of all contributors. The Meso-NH project is the achievement of a much larger team. Our thanks extend to all those who are not cited here, but have given their best to create this unique tool.

Philippe Bougeault and Patrick Mascart

Since the 2002 edition, in addition to the contributors cited above, thanks have to be extended to C. Augros, F. Auguste, D. Barbary, C. Barthe, S. Berthet, Y. Bouteloup, C. Bovalo, O. Caumont, J.-P. Chaboureau, M. Chong, A. Costes, F. Couvreux, T. Dauhut, G. Delautier, J. Escobar, O. Geoffroy, P.A. Joulin, C. Lac, P. Le Moigne, M. Leriche, Q. Libois, T. Lunet, M. Mandement, T. Marić, G. Molinié, T. Nagel, J., O. Nuissier, Pergaud, D. Ricard, Q. Rodier, R. Schoetter, F. Solmon, O. Thouron, M. Tomasini, B. Tsenova, B. Vié and F. Visentin.

Jean-Pierre Chaboureau

Chapter 1

Initial Fields for Idealized Flows

Contents

In many occasions, we want to run simulations starting from highly idealized conditions, such as an atmosphere in geostrophic equilibrium, with simple vertical and horizontal structure, and simple orography, or no orography at all. This is useful for theoretical research on geophysical flows, or simply to test if recent changes in the code have not been detrimental to the quality of previous results. Meso-NH possesses a general program to prepare initial data for such experiments, named PREP_IDEAL_CASE.

This program reads data on the vertical structure of the atmosphere from an input file, that may take a variety of formats for convenience, and prepares a file containing a 2D or 3D initial state satisfying the geostrophic and anelastic balances, according to various specifications for the geographical setting. It is also possible to prepare non balanced fields following simple mathematical formulas, in order to test the good functioning of the post-processing and graphical facility (see last section).

The fields are produced either for a Cartesian geometry, or for a conformal projection. A stretched vertical grid may be used, but only regular horizontal grids are supported in this program. The orography can be zero everywhere, or defined by simple bell-shaped or sine-shaped mountains.

1.1 Input atmospheric profile

The input atmospheric profile may be specified in several ways, depending on the willingness of the user to use observations (or pseudo observations) in various formats, or to achieve a highly idealized experiment.

Sounding formats (Option: 'RSOU')

If one wishes to use observations or pseudo-observations, the most convenient way to communicate with the program is to use one of several available "sounding" formats. The data consist of surface level information, followed by nu levels of temperature and moisture data, and nm levels of wind data. The date and time of the observation must also be supplied.
The following data formats are supported, and may be selected by specification of the appropriate value for the parameter YKIND:

- 'STANDARD' :
  - altitude, pressure, temperature and dew point temperature at ground level,
  - nu levels with pressure, wind direction and wind force,
  - and nm levels with pressure, temperature and dew point temperature.
- 'PUVTHVMR' :
  - altitude, pressure, virtual potential temperature and vapor mixing ratio at ground level,
  - nu levels with pressure, zonal wind component, meridian wind component,
  - nm levels with pressure, virtual potential temperature and vapor mixing ratio.
- 'PUVTHVHU' :
  - altitude, pressure, virtual potential temperature and relative humidity at ground level ,
  - nu levels with pressure, zonal wind component, meridian wind component,
  - nm levels with pressure, virtual potential temperature and relative humidity
- 'ZUVTHVHU' :
  - altitude, pressure, virtual potential temperature and relative humidity at ground level,
  - nu levels with altitude, zonal wind component, meridian wind component,
  - nm levels with altitude, virtual potential temperature and relative humidity.
- 'ZUVTHVMR' :
  - altitude, pressure, virtual potential temperature and vapor mixing ratio at ground level,
  - nu levels with altitude, zonal wind component, meridian wind component,
  - nm levels with altitude, virtual potential temperature and vapor mixing ratio.
- 'PUVTHDMR' :
  - altitude, pressure, dry potential temperature and vapor mixing ratio at ground level,
  - nu levels with pressure, zonal wind component, meridian wind component,
  - nm levels with pressure, dry potential temperature and vapor mixing ratio.
- 'PUVTHDHU' :
  - altitude, pressure, dry potential temperature and relative humidity at ground level,
  - nu levels with pressure, zonal wind component, meridian wind component,

  - nm levels with pressure, dry potential temperature and relative humidity.

- 'ZUVTHDMR' :
  - altitude, pressure, dry potential temperature and vapor mixing ratio at ground level,
  - nu levels with altitude, zonal wind component, meridian wind component,
  - nm levels with altitude, dry potential temperature and vapor mixing ratio.

- 'PUVTHU' :
  - altitude, pressure, temperature and relative humidity at ground level,
  - nu levels with pressure, zonal wind component, meridian wind component,
  - nm levels with pressure, temperature and relative humidity.

More idealized format (Option: 'CSTN')
A more idealized manner to communicate with the program is to assume that the atmosphere is composed of an arbitrary number $n-1$ of layers defined by their altitudes $Z(k)$. Within each layer, the stability is constant, and the wind and relative humidity vary linearly with height. In that case, the input data consist in the surface level information, followed by the moist Väisälä frequency of each layer N_v, and the wind components and relative humidity at the layer interfaces. The virtual potential temperature on the n input levels is retrieved from the N_v data by

$$\theta_v(k) = \theta_v(k-1) \exp\left\{ \frac{N_v^2(k-1)}{g} \left(Z(k) - Z(k-1)\right) \right\} \tag{1.1}$$

for $k = 2, n$. The situation concerning input data is then the same as for the 'ZUVTHVHU' case in the 'RSOU' option, and subsequent treatment is similar.

Specifying a jet structure
For other applications, one may want to have a jet structure $U(y,z)$ instead of a horizontally uniform wind $U(z)$. Then we directly prescribe through a Fortran function the following value of the x-component wind U(y,z):

$$U(\hat{y},\hat{z}) = \frac{1}{\cosh\left(\left(\frac{\hat{y}-\hat{y}_0}{zwidthy}\right)^2 + \left(\frac{\hat{z}-\hat{z}_0}{zwidthz}\right)^2 \right)} \tag{1.2}$$

where $zwidthy$ and $zwidthz$ are the characteristic sizes of the jet along the horizontal and vertical directions. $\hat{y}_0$ and $\hat{z}_0$ are the curvilinear coordinates for the jet center.
An intermediate case is also available where the function U(y,z) is a separable function of y and z:

$$U(y,z) = U(z) * f(y)$$

The vertical part $U(z)$ is still obtained from the input atmospheric profile and the horizontal part $f(y)$ is given by a Fortran function:

$$f(\hat{y}) = \frac{1}{\cosh\left(\frac{\hat{y}-\hat{y_0}}{zwidth}\right)} \tag{1.3}$$

with the same notations as for the jet case.

The jet structure or the separable function, can also be taken into account for the V(x,z). All combinations between U(y,z) and V(x,z) (function of only z, separable or non-separable function) are possible.
All these options lead to the prescription of the wind components along vertical planes (I,K) for V(x,z) and (J,K) for U(y,z) and subsequent treatments to balance the wind and the mass fields are the same.

1.2 Add an orography

An orography following simple form can be specified:
It may be sine shaped:

$$z_s(i,j) = h_{max} \left\{ \sin\left(\frac{\pi i}{IU-1} \right)^2 \right\}^{exp_x} \left\{ \sin\left(\frac{\pi j}{JU-1} \right)^2 \right\}^{exp_y}$$

or bell-shaped :

$$z_s(i,j) = h_{max} / \left\{ 1 + \left(\frac{x(i)-x_s}{a_x} \right)^2 + \left(\frac{y(j)-y_s}{a_y} \right)^2 \right\}^{1.5}$$

IU and JU are the total number of points along x and y directions (i.e. including the external points). h_{max}, exp_x, exp_y, a_x, a_y,x_s and y_s are the degrees of freedom. h_{max} is the maximum height, a_x and a_y represent widths along x and y directions, x_s and y_s are the center positions of the mountain.

1.3 Wind and mass fields on the model grid

To take into account the difference between the orography of the vertical profile and the orography of the MESONH grid, the variables are subject to a "shifting" process as in PREP_REAL_CASE program.
The different grid used in MESONH in PREP_REAL_CASE program are described at section 3.4. In PREP_IDEAL_CASE program, the mixed grid is the Gal-Chen-Sommerville grid with the same $\widehat{z}$ levels as the Meso-NH grid and the orography of the input atmospheric profile. The other grids are defined as in PREP_REAL_CASE program.

Vertical profile on the mixed grid
For the CSTN case, the program will first convert the vertical profile in a common format, featuring only the surface altitude, pressure, virtual temperature and vapor mixing ratio, together with the altitudes of the data points, and the corresponding values of θ_v, r_v, and wind components. For the RSOU case, the program will convert in θ_l, r_t, and wind components.
The correspondance between pressure and altitude is achieved, when necessary, by integration of the hydrostatic relation, starting from the surface level:

$$d\Pi = -\frac{g}{C_{pd}\theta_v} dz \tag{1.4}$$

with $P = P_{00}\Pi^{C_{pd}/R_d}$.

The virtual temperature is obtained as

$$T_v = \theta_v \Pi = \theta_v \left(\frac{P}{P_{00}} \right)^{R_d/C_{pd}} \tag{1.5}$$

In some cases, this requires the use of an iterative procedure to derive the absolute temperature and the vapor mixing ratio from available information (virtual temperature and relative humidity). This is done independantly for each level, and comprises the following steps, starting with $T = T_v$ as first guess:

1. The saturation vapor pressure $e_s(T)$ at temperature T is computed:

$$e_s(T) = \exp\left(\alpha_w - \frac{\beta_w}{T} - \gamma_w \ln(T) \right)$$

   with

$$\begin{aligned} \alpha_w &= \ln(e_s(T_t)) + \frac{\beta_w}{T_t} + \gamma_w \ln(T_t) \\ \beta_w &= \frac{L_v(T_t)}{R_v} + \gamma_w T_t \\ \gamma_w &= \frac{C_l - C_{pv}}{R_v} \end{aligned}$$

   where T_t is the triple point temperature.

2. The partial pressure of the vapor $e = e_s(T_d)$ is computed from the relative humidity Hu (in percents) and the saturation vapor pressure $e_s(T)$:

$$e = \frac{Hu}{100} e_s(T)$$

3. The vapor mixing ratio is evaluated by:

$$r_v = \frac{R_d}{R_v} \frac{e}{P - e}$$

4. The temperature is deduced:

$$T = T_v \frac{(1 + r_v)}{(1 + \frac{R_v}{R_d} r_v)}$$

The iteration continues until convergence is achieved.
Once the variables are known on data points, they are linearly interpolated to the mixed grid. In the RSOU case, θ_l and r_t are then convert in θ_v and r_v with an adjustement procedure. Here θ_v and r_v are located on the mass points of the grid, but the wind components are located on w points. They will be called hereafter U and V. The next sections explain how the 3D fields are produced, starting from this single profile.

Wind and mass fields on the mixed grid

The vertical profile obtained above is supposed to be valid at the point $ILOC, JLOC$ of the horizontal model grid, and we want to reconstitute the whole 3D fields. As a first step in this computation, the program computes the mass fields on a mixed 3D grid to be the same as the vertical profile in all the points of the horizontal grid.
The wind is first projected on to model axes. At this stage, the desired jet structure is introduced to compute the 3D field.

Wind and mass fields on the model grid
Then the shifting process is compute as in PREP_REAL_CASE program.

1.4 Reference state

The reference state is computed on the reference grid, as the horizontal average of the actual state. First, $\theta_{v\,ref}$ and $r_{v\,ref}$ are computed as a mean value at constant altitude of the θ_v and r_v field, after interpolation to the reference grid.
Π^{top}_{ref} is computed as the horizontal average of $\Pi^{top}(x, y)$. Then, the hydrostatic relation for the reference state is integrated from top to bottom to compute Π_{ref}.

$$d\Pi_{ref} = -\frac{g}{C_{pd}\theta_{v\,ref}} dz \tag{1.6}$$

Finally, the density of dry air for the reference state is retrieved

$$\rho_{d\,ref} = \frac{P_{00}(\Pi_{ref})^{R_d/C_{pd}-1}}{R_d\theta_{v\,ref}(1 + r_{v\,ref})} \tag{1.7}$$

1.5 Enforcement of the anelastic constraint

Obviously, wind field obtained at this stage does not fulfil the anelastic constraint (Eq. 2.14 in Part I: Dynamics) and the free-slip boundary conditions. Therefore, a last adjustement is necessary so that this wind field can be used as initial field for the Meso-NH model. Thus, a perturbation deduced from a potential Pot gradient is added to the wind component $\boldsymbol{U}_0$ so that the resulting wind field $\boldsymbol{U}$ satisfies the anelastic constraint.
Let us write this constraint:

$$\boldsymbol{U} = \boldsymbol{U}_0 - \boldsymbol{\nabla} Pot$$
$$\boldsymbol{\nabla}.(\rho_{dref}\boldsymbol{U}) = 0$$

From these 2 equations, we deduce an equation for the Pot field given by:

$$\boldsymbol{\nabla}.(\rho_{dref}\boldsymbol{\nabla} Pot) = \boldsymbol{\nabla}.(\rho_{dref}\boldsymbol{U}_0) \tag{1.8}$$

This equation is equivalent to the pressure equation solved in the temporal loop of the model to determine the pressure function. Therefore, the same iterative solver is used to solve the equation (1.8) and the gradient of this potential is added to find the final field $\boldsymbol{U}$ satifying the anelastic constraint.

1.6 Add a perturbation

In order to start a non-trivial experiment, it is often useful to add a perturbation to the previously defined balanced fields. Two possibilities are presently available:

- add a perturbation to the θ field (convective bubble)

$$Dist = \sqrt{\left(\left(\frac{\hat{x}-\hat{x}_0}{Rad_x}\right)^2 + \left(\frac{\hat{y}-\hat{y}_0}{Rad_y}\right)^2 + \left(\frac{\hat{z}-\hat{z}_0}{Rad_z}\right)^2\right)}$$
$$\theta' = Ampli \cos^2\left(\frac{\pi}{2} Dist\right) \quad \text{for } Dist < 1$$
$$\theta' = 0 \qquad \text{elsewhere}$$

- add a non-divergent perturbation to the horizontal wind, through the use of a streamfunction Φ':

$$\Phi' = Ampli \;\; e^{\left(\frac{\hat{y}-\hat{y}_0}{Rad_y}\right)^2} \;\; \cos\left(\frac{2\pi\hat{x}}{Rad_x}\right)$$

  This streamfunction is located at the vertical vorticity point and the u' and v' perturbations are computed at the right locations by:

$$u' = -\frac{\partial \Phi'}{\partial \hat{y}}$$
$$v' = +\frac{\partial \Phi'}{\partial \hat{x}}$$

  The discretizations use the grid-point curvilinear $\hat{x}, \hat{y}$ because at this point, the orography has not yet being introduced in the model. This guarantees that the perturbation does not change the divergence of the previously obtained fields.

1.7 Analytical 3D fields

For the purpose of testing the post-processing and graphical facility, it is also possible to generate a family of simple 3D analytical fields. Three types of such fields are possible: spherical fields, plane fields and wave fields.

- spherical fields:

$$\overline{\rho^*}^x \mathcal{U} = \overline{\rho^*}^x \left\{ f_0 + 0.5(f_1 - f_0)\sqrt{\frac{x-x_0}{L_x} + \frac{y_m-y_0}{L_y} + \frac{z_m-z_0}{L_z}} \right\} \tag{1.9}$$

$$\overline{\rho^*}^y \mathcal{V} = \overline{\rho^*}^y \left\{ f_0 + 0.5(f_1 - f_0)\sqrt{\frac{x_m-x_0}{L_x} + \frac{y-y_0}{L_y} + \frac{z_m-z_0}{L_z}} \right\} \tag{1.10}$$

$$\overline{\rho^*}^z w = \overline{\rho^*}^z \left\{ f_0 + 0.5(f_1 - f_0)\sqrt{\frac{x_m-x_0}{L_x} + \frac{y_m-y_0}{L_y} + \frac{z-z_0}{L_z}} \right\} \tag{1.11}$$

$$\rho^* \theta(k) = \rho^* \left\{ f_0 + 0.5(f_1 - f_0)\sqrt{\frac{x_m-x_0}{L_x} + \frac{y_m-y_0}{L_y} + \frac{z_m-z_0}{L_z}} \right\} \tag{1.12}$$

$$\rho^* r_n = 0. \tag{1.13}$$

- plane fields :

$$\overline{\rho^*}^x \mathcal{U} = \overline{\rho^*}^x \left\{ f_0 + (f_1 - f_0) \left(\frac{x - x_0}{L_x} N_x + \frac{y_m - y_0}{L_y} N_y + \frac{z_m - z_0}{L_z} N_z \right) \right\} \quad (1.14)$$

$$\overline{\rho^*}^y \mathcal{V} = \overline{\rho^*}^y \left\{ f_0 + (f_1 - f_0) \left(\frac{x_m - x_0}{L_x} N_x + \frac{y - y_0}{L_y} N_y + \frac{z_m - z_0}{L_z} N_z \right) \right\} \quad (1.15)$$

$$\overline{\rho^*}^z w = \overline{\rho^*}^z \left\{ f_0 + (f_1 - f_0) \left(\frac{x_m - x_0}{L_x} N_x + \frac{y_m - y_0}{L_y} N_y + \frac{z - z_0}{L_z} N_z \right) \right\} \quad (1.16)$$

$$\rho^* \theta(k) = \rho^* \left\{ f_0 + (f_1 - f_0) \left(\frac{x_m - x_0}{L_x} N_x + \frac{y_m - y_0}{L_y} N_y + \frac{z_m - z_0}{L_z} N_z \right) \right\} \quad (1.17)$$

$$(1.18)$$

$$\rho^* r_n = 0. \quad (1.19)$$

where

$$N_x = \cos(\alpha_z)\sin(\alpha_x) \quad (1.20)$$

$$N_y = -\cos(\alpha_z)\cos(\alpha_x) \quad (1.21)$$

$$N_y = -\sin(\alpha_z) \quad (1.22)$$

- wave fields:

$$\overline{\rho^*}^x \mathcal{U} = \overline{\rho^*}^x \left\{ f_0 + (f_1 - f_0) \left(\frac{x - x_0}{L_x} N_x + \frac{y_m - y_0}{L_y} N_y + \frac{z_m - z_0}{L_z} N_z \right) \right. \quad (1.23)$$

$$\left. + \; 0.125(f_1 + f_0) \sin \left(2\pi f_2 (\frac{x - x_0}{L_x} C_s + \frac{y_m - y_0}{L_y} S_n) \right) \right\} \quad (1.24)$$

$$\overline{\rho^*}^y \mathcal{V} = \overline{\rho^*}^y \left\{ f_0 + (f_1 - f_0) \left(\frac{x_m - x_0}{L_x} N_x + \frac{y - y_0}{L_y} N_y + \frac{z_m - z_0}{L_z} N_z \right) \right. \quad (1.25)$$

$$\left. + \; 0.125(f_1 + f_0) \sin \left(2\pi f_2 (\frac{x_m - x_0}{L_x} C_s + \frac{y - y_0}{L_y} S_n) \right) \right\} \quad (1.26)$$

$$\overline{\rho^*}^z w = \overline{\rho^*}^z \left\{ f_0 + (f_1 - f_0) \left(\frac{x_m - x_0}{L_x} N_x + \frac{y_m - y_0}{L_y} N_y + \frac{z - z_0}{L_z} N_z \right) \right. \quad (1.27)$$

$$\left. + \; 0.125(f_1 + f_0) \sin \left(2\pi f_2 (\frac{x_m - x_0}{L_x} C_s + \frac{y_m - y_0}{L_y} S_n) \right) \right\} \quad (1.28)$$

$$\rho^* \theta(k) = \rho^* \left\{ f_0 + (f_1 - f_0) \left(\frac{x_m - x_0}{L_x} N_x + \frac{y_m - y_0}{L_y} N_y + \frac{z_m - z_0}{L_z} N_z \right) \right. \quad (1.29)$$

$$\left. + \; 0.125(f_1 + f_0) \sin \left(2\pi f_2 (\frac{x_m - x_0}{L_x} C_s + \frac{y_m - y_0}{L_y} S_n) \right) \right\} \quad (1.30)$$

$$(1.31)$$

$$\rho^* r_n = 0. \quad (1.32)$$

where

$$C_s = \cos(\alpha_x)$$

$$S_n = \sin(\alpha_x)$$

$f_0, f_1, f_2, \alpha_x, \alpha_z$ are the degrees of freedom. L_x, L_y,L_z are the lengths of the physical part of the domain. x_0, y_0 and z_0 represent the coordinates of the center point of the physical part of the domain.

Chapter 2

Forced Mode Version

Contents

2.1 Purpose

For some academic studies (1D PBL dynamics, 2D Eady wave problem, 2D mountain flow, moving squall lines, 3D breeze studies...), it is necessary to impose a large scale environment even crudely (geostrophic wind, subsidence, ...), in order to perform consistent simulations with Meso-NH. Practically, this means that some additional forcing terms have to be included in the Meso-NH system of equation.
Actually, only the most usual physical forcing terms have been taken into account for simplicity. The forcing terms are prescribed empirically from external sources of information (e.g. series of observation) and are mutually independent when acting on the same prognostic variable. Generally they are non-stationary and horizontally homogeneous, only the case of flat terrain is addressed. Furthermore, forcing terms are considered for the restricted Cartesian geometry of Meso-NH (constant Coriolis parameter).
The effects of several forcings are considered:

- Domain translation at a constant speed:
(affects the surface fluxes and the Coriolis force)

- Geostrophic wind (or pressure gradient) forcing:
$$\left.\frac{\partial u}{\partial t}\right|_{FRC} = +f v_{frc}$$
$$\left.\frac{\partial v}{\partial t}\right|_{FRC} = -f u_{frc}$$

• Forced ascent or descent (vertical transport) of α:
applied to all prognostic variables (w excepted in the 1D case)
$$\left.\frac{\partial \alpha}{\partial t}\right|_{FRC} = -w_{frc}\frac{\partial \alpha}{\partial z}$$

• Large scale horizontal transport of $\alpha \in [\theta, r_v]$:
$$\left.\frac{\partial u}{\partial t}\right|_{FRC} = -u(\frac{\partial \alpha}{\partial x})_{frc}$$
$$\left.\frac{\partial v}{\partial t}\right|_{FRC} = -v(\frac{\partial \alpha}{\partial y})_{frc}$$

• Large scale variables $\alpha \in [u, v, \theta, r_v]$:
for a Newtonian relaxation with damping time τ_{frc}
$$\left.\frac{\partial \alpha}{\partial t}\right|_{FRC} = -\frac{\alpha - \alpha_{frc}}{\tau_{frc}}$$

In the above definitions, the subscript $_{frc}$ tags the forcing fields or scalars which must be provided by the user for a specific application. The forcing terms are written in the form of a tendency of the relevant prognostic variable.

2.2 Modified equations

The inclusion of the forcing terms (single underbraced for the physical terms and double underbraced for the Newtonian relaxation terms) in the Meso-NH system of equation is made as follows:

Conservation of momentum

$$\frac{\partial}{\partial t}(\rho_{dref}\boldsymbol{U}) \quad + \boldsymbol{\nabla}\cdot(\rho_{dref}\boldsymbol{U}\otimes\boldsymbol{U}) + \rho_{dref}\boldsymbol{\nabla}\Phi + \rho_{dref}\boldsymbol{g}\frac{\theta_v - \theta_{vref}}{\theta_{vref}} + 2\rho_{dref}\boldsymbol{\Omega}\wedge(\boldsymbol{U} - \underbrace{\boldsymbol{U}_{frc}}) + \underbrace{w_{frc}\frac{\partial u}{\partial z}\boldsymbol{i}} + \underbrace{w_{frc}\frac{\partial v}{\partial z}\boldsymbol{j}} = \rho_{dref}\boldsymbol{\mathcal{F}} - \underbrace{\underbrace{\frac{u - u_{frc}}{\tau_{frc}}\boldsymbol{i}}} - \underbrace{\underbrace{\frac{v - v_{frc}}{\tau_{frc}}\boldsymbol{j}}} \tag{2.1}$$

Thermodynamic equation

$$\frac{\partial}{\partial t}(\rho_{dref}\theta) + \boldsymbol{\nabla}\cdot(\rho_{dref}\theta\boldsymbol{U}) + \rho_{dref}\Big(\underbrace{u(\frac{\partial\theta}{\partial x})_{frc}} + \underbrace{v(\frac{\partial\theta}{\partial y})_{frc}} + \underbrace{w_{frc}\frac{\partial\theta}{\partial z}}\Big) = \rho_{dref}\Big[\frac{R_d + r_v R_v C_{pd}}{R_d C_{ph}} - 1\Big]\frac{\theta}{\Pi_{ref}}w\frac{\partial\Pi_{ref}}{\partial z} + \frac{\rho_{dref}}{\Pi_{ref}C_{ph}}\Big[L_m\frac{D(r_i + r_s + r_g + r_h)}{Dt} - L_v\frac{Dr_v}{Dt} + \mathcal{H}\Big] - \underbrace{\underbrace{\frac{\theta - \theta_{frc}}{\tau_{frc}}}} \tag{2.2}$$

Conservation of the water vapor mixing ratio

$$\frac{\partial}{\partial t}(\rho_{dref}r_v) + \boldsymbol{\nabla}\cdot(\rho_{dref}r_v\boldsymbol{U}) + \rho_{dref}\Big(\underbrace{u(\frac{\partial r_v}{\partial x})_{frc}} + \underbrace{v(\frac{\partial r_v}{\partial y})_{frc}} + \underbrace{w_{frc}\frac{\partial r_v}{\partial z}}\Big) = \rho_{dref}Q_v - \underbrace{\underbrace{\frac{r_v - r_{v\,frc}}{\tau_{frc}}}} \tag{2.3}$$

Conservation of the condensed water mixing ratios

$$\frac{\partial}{\partial t}(\rho_{dref}r_\star) + \boldsymbol{\nabla}\cdot(\rho_{dref}r_\star\boldsymbol{U}) + \rho_{dref}\underbrace{w_{frc}\frac{\partial r_\star}{\partial z}} = \rho_{dref}Q_\star \tag{2.4}$$

These forced terms are not independent from each other, the horizontal gradient of θ (baroclinicity) is related to the geostrophic wind by the "thermal wind" equation which takes the following form:

$$\frac{\partial u_{frc}}{\partial z} = +\frac{g}{f\theta_{vref}}(\frac{\partial \theta_v}{\partial y})_{frc} \tag{2.5}$$

$$\frac{\partial v_{frc}}{\partial z} = -\frac{g}{f\theta_{vref}}(\frac{\partial \theta_v}{\partial x})_{frc} \tag{2.6}$$

where u_{frc} and v_{frc} are the horizontal components of the geostrophic wind and $f = 2\boldsymbol{\Omega} \cdot \boldsymbol{k}$, the (constant) Coriolis parameter.
The forced temperature gradients are deduced from these relations but beware that condensation modifies gradients of θ or r_v and so forced gradients of θ or forced advection of humidity might be excessive in some circumstances.
The relaxation towards large scale variables is useful to constraint a free atmosphere state to match series of observation above a specified height level.

2.3 Interpolation

The series of asynchronous 1D forcing data are provided by the Meso-NH user in a special format (see the **Forced version** described in the **Meso-NH user's guide**). Then they are linearly interpolated to fill the Meso-NH vertical grid system and stored in the LFI files. In the case of orography, these fields are further projected on the horizontal embedded grids of Meso-NH by linear interpolation.
The time-evolution of the forcings is obtained by linear interpolation between two bounding forcing fields at each time step. When the last forcing data is reached a stationary forcing is kept on. Conversely, no forcing is applied until the current time of the Meso-NH integration has reached that of the first forcing data. The following scheme summarizes how a set of 3 forcing data are used during the model integration starting at time DTEXP.

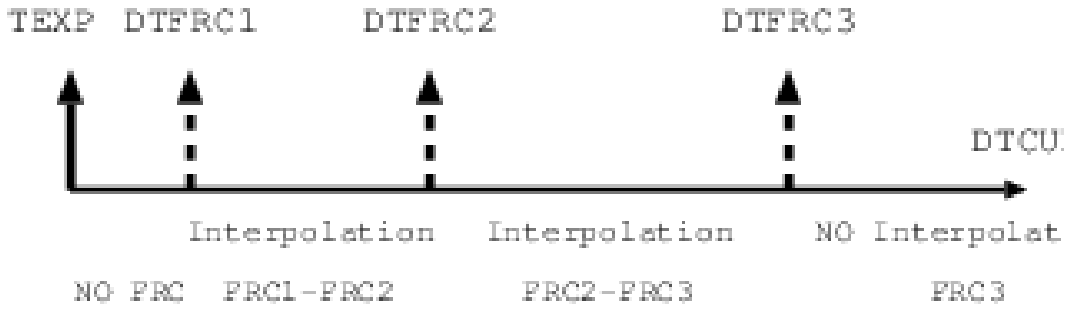

2.4 Discretization

The vertical transport $w_{frc}(\frac{\partial \alpha}{\partial z})$ is lagged and integrated with a first order upstream scheme to ensure positivity in some situation, e.g. the case of large scale subsidence over a shallow inversion in the stratus cloud modeling problem. The numerical scheme of the large scale horizontal transport

is time centered and the horizontal forcing gradients $(\frac{\partial \alpha}{\partial x})_{frc}$ and $(\frac{\partial \alpha}{\partial y})_{frc}$ are assumed to be given on the α (mass) grid. The integration of the large scale relaxation terms is lagged for numerical stability. This term applies either above a constant selected height or above a time evolving thermal inversion (useful for PBL dynamics studies).

Chapter 3

Initial Fields for Real Flows

Contents

3.1 General presentation

The simulation of realistic meteorological situations is an important scope of Meso-NH. The preparation of initial and coupling (LB and LS) fields by interpolation of larger-scale meteorological analyses or forecasts, in a format ready to start a Meso-NH experiment, is therefore an important task. These may be produced from any situation contained in the ECMWF or Meteo-France operational archive (including the special reanalyses projects). A Meso-NH file, coming from a simulation at lower resolution, can also be used as larger-scale model, to provide initial fields - including finer surface fields and orography - for a Meso-NH run at higher resolution

(with or without *gridnesting* technique). This gives access to a wealth of possibilities.

3.1.1 Initialization for a one-model run, from operationel models

This type of model simulation uses one initial file (with all the fields at beginning time of the simulation), and a certain number of coupling files to prescribe the lateral boundary conditions to the model at further time steps. The coupling files are of the same nature than the initial file. Here is presented the way to produce these initial and coupling files.

This sequence for real cases contains three procedures or programs (Fig. 3.1). In the following, a Fortran program is written in CAPITAL letters, and is run with the Meso-NH procedure *prepmodel* (Unix procedure written in lower case letters).

1. PREP_PGD: this Meso-NH program computes the physiographic data file (called PGD file below). At this step, you choose the projection, resolution, and horizontal domain. The PGD file contains all the physiographic data necessary to run the Meso-NH model with interactive surface schemes for vegetation and town.

2. *extractecmwf*[1] or *extractarpege*: these two friendly procedures extract the surface and altitude fields for one date, respectively from MARS archive (ECMWF forecast model) or from Meteo-France operational archive (ARPEGE and ALADIN models). In both cases, the fields are written in a GRIB format file, on the Gaussian grid. The extraction must be done separately for each date and time (for the initial file and each of the coupling file).

3. PREP_REAL_CASE: this Meso-NH program performs the change of orography and vertical grid and writes the Meso-NH file, which will be used either for the beginning of the simulation or for coupling.

3.1.2 Initialization for a one-model run, from a Meso-NH file

In this case, the initial and coupling files are interpolated from a previous Meso-NH run (at coarser resolution). It is again necessary to produce separately one initial file and the coupling files. The following steps are used (Fig. 3.2):

1. PREP_PGD

2. SPAWNING: this program performs the horizontal interpolations from a Meso-NH file into another Meso-NH file, with a finer resolution and smaller domain.

3. PREP_REAL_CASE

3.1.3 Initialization for a nesting run

Two or more Meso-NH models will be run interactively. The first model, the one with the coarser resolution and containing the others, needs again one initial file and some coupling files (for lateral boundary conditions).

[1] A user is necessary on the station ecaccess of Reading to run *extractecmwf*

However, the nested models are contained in another Meso-NH model. This allows to give them their lateral boundary conditions directly interpolated from the model which contains it, at all time-steps. Therefore, no coupling file is necessary for those models. The initial file must still be computed before the run (the interpolation program for all the model fields is not yet included in the model program itself).
The user can choose the date of the nested model start as he wants (it is not necessary the same than the coarser model). The only obligation is to start a nested model only if all the coarser models containing it have already started, or are starting.

The initialisation sequence is a merging of the two previous ones (initialisation and coupling files of the first model; initialisation files from Meso-NH model for the nested files). However, there is a **major change** at the beginning of the sequence: **all the PGD files for all models must be computed before the PREP_REAL_CASE program** (and as a consequence before the first model run). These PGD files are then checked, and conformity between them for gridnesting is imposed - the orography of one model in every grid mesh is set equal to the average of any of its nested model orography on the same area.
The initialisation and gridnesting sequence is shown here for three models, model 2 included in model 1, and model 3 included in model 2.

1. PREP_PGD: this program is run as many time as the number of models:
   - physiographic data file for the model 1 (including projection, resolution, domain),
   - physiographic data file for the model 2 (including resolution, domain),
   - physiographic data file for the model 3 (including resolution, domain).
2. PREP_NEST_PGD: this program checks all the PGD files at the same time, and imposes the conformity between them.
3. *extractecmwf* or *extractarpege*: it extracts the surface and altitude fields for one date, for model 1. The extraction must be done separately for each date and time (for the initial file and each coupling file).
4. PREP_REAL_CASE: this program is run several times, for the initial file and the coupling files of model 1.
5. MESONH: this step is **optional**. If you do not wish to start all the models at the same time, you can decide to run the model 1 before the model 2 starts.
6. SPAWNING: when you want to start the model 2, you must use this program to compute the horizontal interpolations from the model 1 to the model 2. It is used only once.
7. PREP_REAL_CASE: It is used only once, to compute the initial file for the model 2. **Do not change the vertical grid**.
8. MESONH: again, this step is **optional**. If you do not wish to start all model 3 at the same time as model 2, you can decide to run the models 1 and 2 alone before.
9. SPAWNING: when you want to start the model 3, you must use this program to compute the horizontal interpolations from the model 2 to the model 3. It is used only once.

10. PREP_REAL_CASE: It is used only once, to compute the initial file for the model 3. **Do not change the vertical grid**.

11. MESONH: here is now your complete nested run.

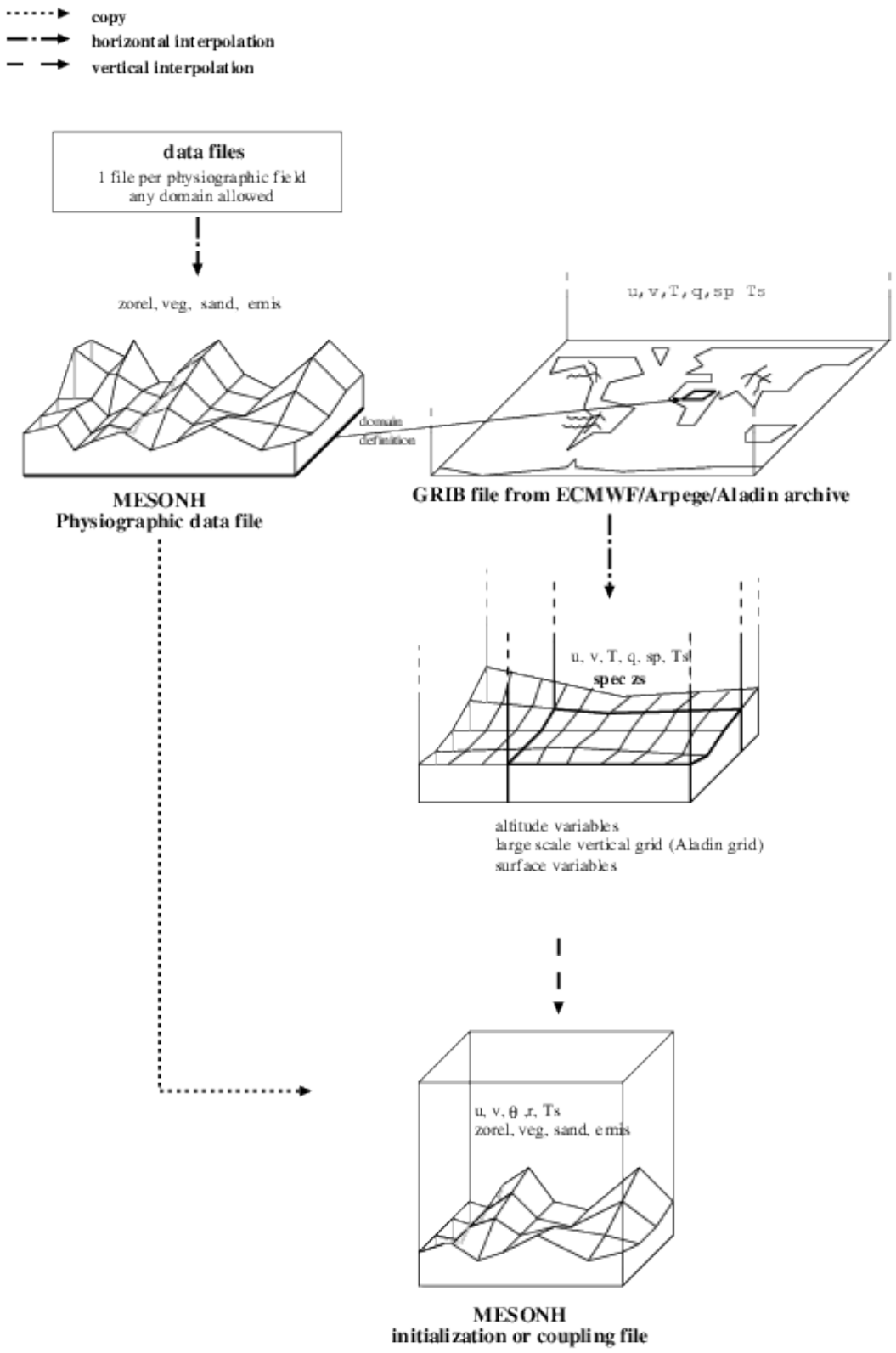

Figure 3.1: schematic view of the interactions between the different files during the initialization sequence of a real case simulation from a global file of ECMWF or METEO-FRANCE archive.

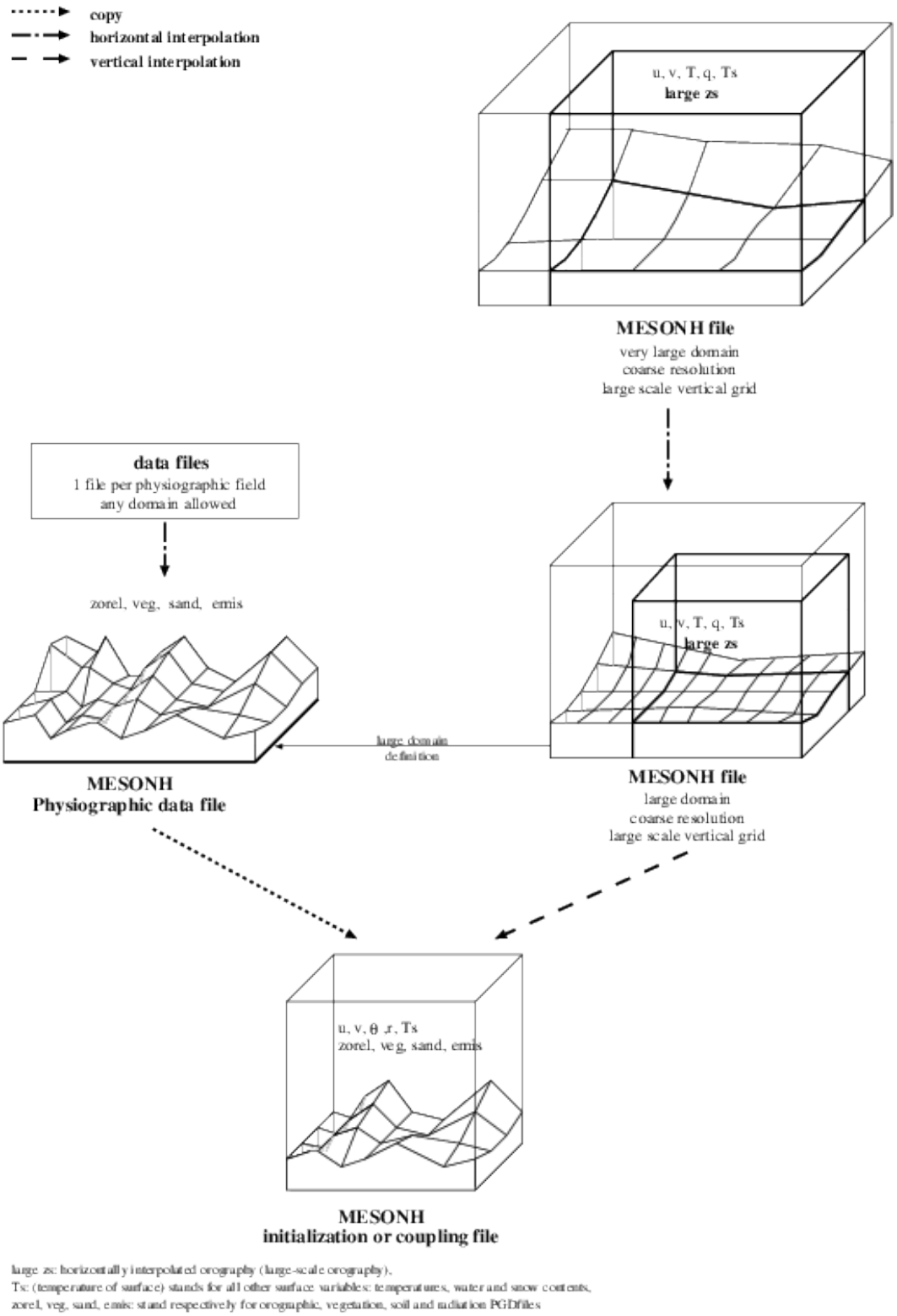

Figure 3.2: schematic view of the interactions between the different files during the initialization sequence of a real case simulation from a Meso-NH file.

3.2 The PREP_REAL_CASE algorithm

The Meso-NH program PREP_REAL_CASE performs the following tasks:

- the horizontal interpolation of the large-scale GRIB data fields (in case of ALADIN, ARPEGE, or ECMWF archive).
- the truncation of the horizontal domain (for convenience, one may want to use very large horizontal domains for the large-scale files (Aladin, Arpege, ECMWF or spawned[2] Meso-NH files), and run Meso-NH on a small fraction only (e.g. for testing).
- the conversion, if necessary, of the prognostic variables of the input files to the prognostic variables of Meso-NH (still on the input - or large scale - grid), and the computation of the altitude of the points of this grid, in order to prepare for the next steps.
- the variables are subject to a special "shifting" process, to take into account the difference between the large-scale and Meso-NH orographies.
- Then the variables are vertically interpolated to the Meso-NH grid.
- Finally, the wind and mass fields are forced to satisfy the anelastic constraint, by one call to the pressure solver, and subsequent modification of the fields.

The resulting Meso-NH file may be used to start a run. In practice, sequences of such files are produced, separated by a few hours. The first file is used to initialize the Meso-NH run, and subsequent files are used to update the boundary conditions and/or the large-scale forcing terms. The remainder of the chapter describes those treatments in detail.

3.3 Horizontal interpolation

3.3.1 Introduction

The first step of PREP_REAL_CASE is the horizontal interpolation of the data fields of the GRIB file (either ECMWF, ALADIN or ARPEGE archive) from the archive grid to the chosen grid.

The following fields are interpolated :

- 3D fields
  - wind component u
  - wind component v
  - absolute temperature T
  - specific humidity q
- 2D ground and under surface fields
  - soil surface temperature

[2] spawned file: file obtained after the Meso-NH to Meso-NH horizontal interpolation program SPAWNING

- sea surface temperature
- deep ground temperature
- surface water content
- deep ground water content
- snow

The next sections of the paragraph present the general interpolation scheme and the specificity of each field.

3.3.2 The interpolation algorithm

The interpolations are performed on the 12 surrounding colocation points (Fig. 3.3), with a first interpolation along the latitudes (with third order polynoms interpolation with 4 points and linear interpolation for 2 points) and a second along the longitude (third order polynoms interpolation):

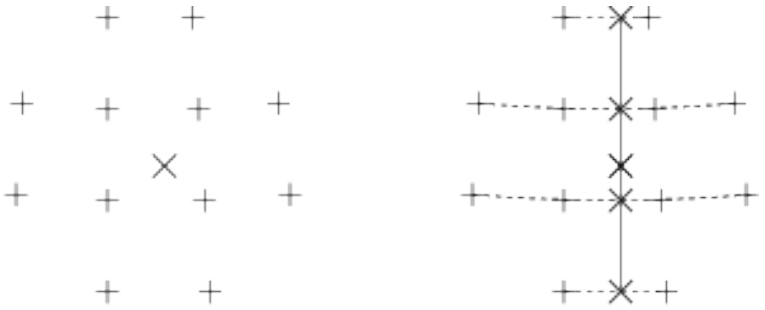

Figure 3.3: Horizontal interpolations in FULL-POS.

Masks may be used for surface fields. In this case, points are interpolated with points of the same nature (mask value). For example, if we are interpolating a point in the sea and we find that from the twelve surrounding points, only eleven are sea points, the interpolation will take only these eleven points into account.
For points which can not be correctly interpolated (points which are not surrounded by enough data points of the same type), a special extrapolation is performed; the given value is the one of the nearest data point of the same type.

3.3.3 Definition of interpolated fields

- Absolute temperature
  From the archived absolute temperature is computed the virtual potential temperature which is interpolated and then converted back to absolute temperature.
  The used formula is the following one:
  $\theta_v = T(\frac{P}{P_0})^{-\frac{R_d}{C_{pd}}} \ (1 + \frac{R_v}{R_d} r_v)/(1 + r_v)$

- Specific humidity
  The relative humidity is computed from the archived specific humidity and the archived absolute temperature using the following formula:
  $H = P\, q\, /(\frac{R_d}{R_v} \epsilon_s(T))$

$\epsilon_s(T) = \exp(\alpha_w - \frac{\beta_w}{T} - \gamma_w \log(T))$
H is interpolated and then the specific humidity is computed back.

- Wind components u and v
  The wind components are read separately and interpolated separately. The interpolation is done on the value found in the archive, the definition vectors of u and v are projected on Meso-NH coordinate system after the interpolation.
  The projection of these vectors depends on the archive grid:

  - ECMWF:
    The grid used is a standard latitude, longitude one. The projection consists of a rotation in the tangent plane. The rotation angle is given by the formula:
    $\alpha = R_{pk}(\lambda - \lambda_0) - \beta$
    where:
    R_{pk} is the projection coefficient of the Meso-NH domain,
    λ is the longitude of the point,
    β is the angle of rotation of the Meso-NH domain.
  - ARPEGE:
    ARPEGE uses a stretched grid, therefore winds have first to be projected on a standard lat,lon grid (projection formulas were given by Meteo-France). The projection is then processed in the same way as for ECMWF.
  - ALADIN:
    Both Meso-NH and ALADIN use conformal projections, then the projection of the wind vector consists of a rotation. The rotation angle is given by formula:
    $\alpha = R_{pk}(\lambda - \lambda_0) - \beta - R_{pk_{ALADIN}}(\lambda - \lambda_{0_{ALADIN}})$

- Soil temperature and sea temperature
  The soil and sea temperature are computed from an interpolation of the surface temperature using a land/sea mask.
  To define if a data point from the archive is a land temperature or a sea temperature, the archive land/sea mask is used. This land/sea mask is not a fraction of land, the values store in the archives are integer. The output points are said to be from land if the PGD land fraction is not null. They are said to be from sea if the PGD land fraction is not equal to 1.
  It should be noted that the mask defining the sea surface temperature and the one used by the soil surface temperature are not complementary.

- Deep ground temperature
  The deep ground temperature is interpolated from the archived value, using the same mask as for the soil temperature.

- Soil and deep soil moisture
  These fields are first converted from specific humidity to relative humidity, the interpolation is performed and then they are converted back into specific humidity.
  The value given are dependent of the soil model chosen for the archive. Therefore they have to be converted to Meso-NH soil model.

- Snow
  Snow is interpolated using the same mask as for soil temperature.

3.4 The different grids

Six grids are used in PREP_REAL_CASE: the first five share the same location of the points on the horizontal, and the last one is a purely vertical grid used for reference state computations (Fig. 3.4).

- **The large-scale grid**: this grid is the one used either in the ALADIN file or large-scale Meso-NH file. In the case of an ALADIN input file, this grid is defined by the hybrid coordinate η, and has L levels. The position of variables on this grid is shown in detail in Fig. 3.5. The index of level on the large scale grid will be called l hereafter.

- **The Meso-NH grid**: this grid is the grid of the output Meso-NH file, which will be used during the Meso-NH simulation for the 3D fields. It has (KE-KB+1) physical levels (see Fig. 3.5), plus some levels under the ground or at and over the model top ($z = H$) for boundary treatments. This grid is defined by the Meso-NH orography and the vertical discretization of the Gal-Chen coordinate $\widehat{z}$. The index of level will be called k hereafter.

- **The mixed grid**: this grid is the Gal-Chen-Sommerville grid with the same $\widehat{z}$ levels as the Meso-NH grid and the large scale orography.

- **The shifted grid**: this grid is the mixed grid on which has been applied the shifting function (see hereafter). Therefore it follows the Meso-NH orography, but it is not a Gal-Chen-Sommerville type grid. It has the same number of levels as the Meso-NH grid, and the levels are known by their altitudes.

- **The profile grid**: this grid is the Gal-Chen-Sommerville grid with the same $\widehat{z}$ levels as the Meso-NH grid and an orography defined as the minimum of both orographies, z_{min}. This grid allows to represent the free-atmosphere θ_v profiles (see hereafter) whose value could be interpolated on every point of both mixed and shifted grids. Note that z_{min} can be negative because of the spectral initial form of the large scale orography (Gibbs phenomenon).

- **The reference grid**: this grid is the Gal-Chen grid, a particular case of the grid above, without orography. This grid is only used for the reference state.

For sake of clarity, the horizontal coordinates of the 3D fields are omitted in the following equations.

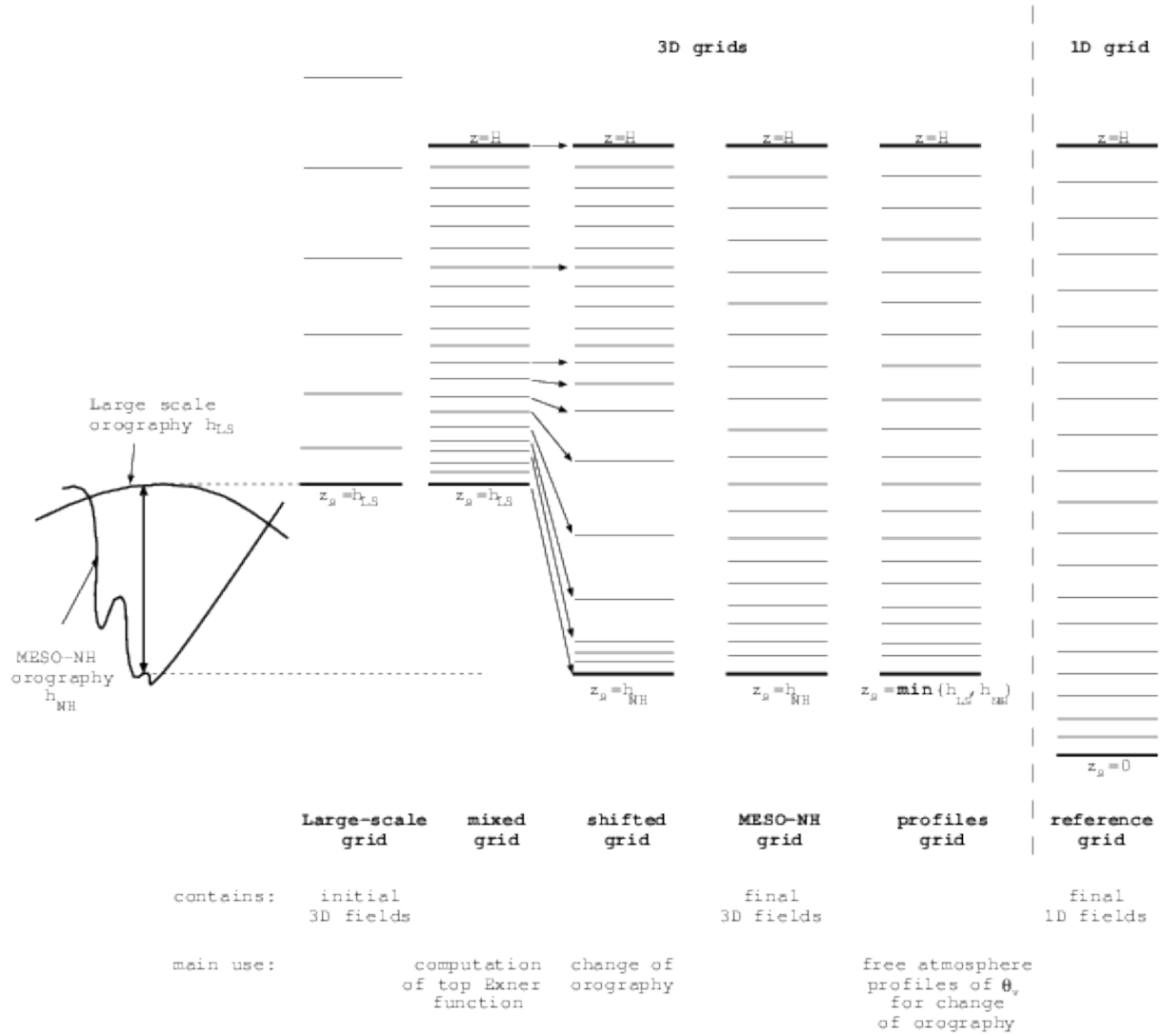

Figure 3.4: The six grids used in PREP_REAL_CASE, shown here for the case where the Meso-NH orography is lower than the large-scale orography.

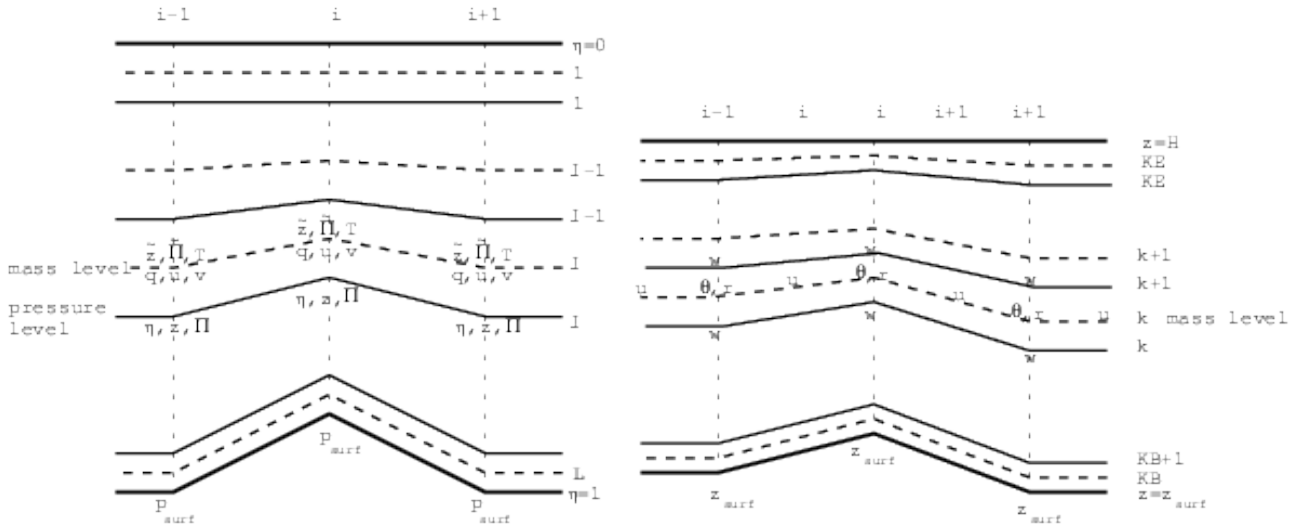

Figure 3.5: ALADIN grid (left) and Meso-NH grid (right). The main 3D-variables used or defined in this chapter are shown, except v in the cross section of the Meso-NH grid because it is located one half-mesh in front of the mass point.

3.5 Altitude of the ALADIN points and conversion of the variables

This step is performed only when the input atmospheric large-scale file is a GRIB one (if the input large-scale file is a Meso-NH one, the variables are directly the correct ones). To preserve the largest accuracy in the hydrostatic balance and the continuity equation through the vertical interpolation process, we want to interpolate the quantities r_v, θ_v, ρu, ρv and w. On the other hand, the GRIB file contains the specific humidity q, the absolute temperature T, and the wind components u and v. All four variables are located on the mass points of the ALADIN grid (Fig. 3.5), therefore the altitudes of those points must also be evaluated as accurately as possible.

Mixing ratio
The mixing ratio of water vapor r_v is readily obtained from the specific humidity q as

$$r_v = \left(\frac{1}{q} - 1\right)^{-1} \tag{3.1}$$

Virtual potential temperature
The virtual temperature at the mass points of the ALADIN grid is readily obtained as

$$T_v = T(1 + r_v R_v/R_d)/(1 + r_v) \tag{3.2}$$

To obtain the virtual potential temperature θ_v, we must know the Exner function Π at the same levels.
Let us call $\tilde{\Pi}_l$ the value of the Exner function at the mass level l of the ALADIN grid, and Π_l the Exner function at the half levels of the same grid. The latter is easy to compute because P is known there:

$$\Pi_l = (\frac{P_l}{P_{00}})^{R_d/C_{pd}} \tag{3.3}$$

Then, we want to preserve the mass in each layer as accurately as possible in the interpolation. We note that the discretization of the hydrostatic relation in the ALADIN file would read with the alternative variables T_v and θ_v

$$z_l - z_{l-1} = -\frac{C_{pd} T_{v_l}}{g} \quad (\ln \Pi_l - \ln \Pi_{l-1}) \tag{3.4}$$

$$z_l - z_{l-1} = -\frac{C_{pd} \theta_{v_l}}{g} \quad (\Pi_l - \Pi_{l-1}) \tag{3.5}$$

This leads to the optimal way of computing

$$\tilde{\Pi}_l = \frac{\Pi_l - \Pi_{l-1}}{\ln \Pi_l - \ln \Pi_{l-1}} \tag{3.6}$$

from which the virtual potential temperature follows

$$\theta_{v_l} = T_{v_l} / \tilde{\Pi}_l \tag{3.7}$$

Altitude of the points of the large-scale grid

Since all variables are located at the mass points of the ALADIN grid, in order to perform the vertical interpolation, one must compute the altitudes of these points.

1) The altitude of each pressure point is given by integration of the hydrostatic relation from bottom to top, discretized as equation (3.5).

2) Assuming a linear variation of θ_v with η, the altitude $\tilde{z}_l$ of the mass point on level l is given by:

$$\tilde{z}_l = z_l - \frac{C_{pd} \left(\frac{3}{4} \theta_{v_l} + \frac{1}{4} \theta_{v_{l+1}} \right)}{g} (\tilde{\Pi}_l - \Pi_l) \tag{3.8}$$

Horiozontal wind components

The wind components are initially contravariant on the ALADIN grid (i.e. following the iso-η surfaces and not true horizontal planes). They are projected onto each true horizontal plane containing the considered point.

Vertical wind components

It is retrieved from the approximated formula of diagnostic vertical velocity in models with η coordinate. If η equal 0 at model top and 1 at ground, and with $p = A(\eta) p_0 + B(\eta) p_s$:

$$\begin{aligned} gw \;=\; & \frac{1}{\rho} \int_0^{\eta} \boldsymbol{\nabla}_{\eta} \left((\frac{dA}{d\eta'} p_0 + \frac{dB}{d\eta'} p_s) \boldsymbol{U} \right) d\eta' \\ & - \frac{B(\eta)}{\rho} \int_0^{1} \boldsymbol{\nabla}_{\eta} \left((\frac{dA}{d\eta'} p_0 + \frac{dB}{d\eta'} p_s) \boldsymbol{U} \right) d\eta' + \frac{\rho_s}{\rho} B(\eta) \boldsymbol{U} \cdot \boldsymbol{\nabla} (g\, z_s) \end{aligned}$$

3.6 Interpolation to the mixed grid

The fields are interpolated to the mixed grid (there is no change of orography). Then, if the chosen vertical grid top is higher than the highest input model one, the program aborts. There is no extrapolation, and therefore, the new vertical grid must not go too high.

Pressure at the model top

The values of Π at the altitude $z = H$ (top of the Meso-NH grid) are determined by vertical integration of the hydrostatic equation from bottom to top (surface pressure is known). This integration is performed on the mixed grid, where all variables have been interpolated, because its

discretization will be approximately the same as the Meso-NH grid (only change of orography). If computed with the ALADIN grid, even with attention paid to mass conservation, one could have for ALADIN levels spaced more than 3 km apart an error of 1 hPa on the surface pressure, when reintegrated with the Meso-NH grid. This error is evident at the model top.
The field of Exner function at model top is hereafter noted $\Pi^{top}(x, y)$. It will be used to compute the total dry mass.

Horizontal momentum
We compute ρ on the mass points of the mixed grid as:

$$\rho_d = \frac{P_{00}(\Pi)^{C_{pd}/R_d - 1}}{R_d \theta_v} \tag{3.9}$$

The values of ρu and ρv follow.

3.7 The shifting process

The next step is to account for the differences in the ALADIN and Meso-NH orographies. There is no standard way of doing this, and the treatment relies on conceptual ideas on the way the flow reacts to the presence of the orography. We also want to preserve some information on the boundary layer structure, inasmuch as possible.
The basic conceptual model is that the whole atmosphere will be vertically displaced (shifted) from the large-scale orography to the Meso-NH orography (Fig. 3.6). The maximum vertical displacement occurs at the ground, where it equals $h_{NH} - h_{LS}$. Further aloft, the displacement diminishes, and is negligible at some height z_{scale} above the ground. So, we define the shifting function

$$f(z) = z + (h_{NH} - h_{LS}) \left(1 - \tanh^2 \left(\frac{z - h_{LS}}{z_{scale}} \right) \right) \tag{3.10}$$

as the vertical displacement experienced by a parcel located at altitude z on the large-scale grid. By default, z_{scale} takes the value of 1000 m.

The next problem is to choose those quantities which will be conserved during the shifting process. This clearly has important consequences: for instance, if r_v and θ_v were conserved, this would generate warm and dry anomalies in the valleys resolved by the Meso-NH orography, and unresolved by the large-scale orography. This is not desirable.

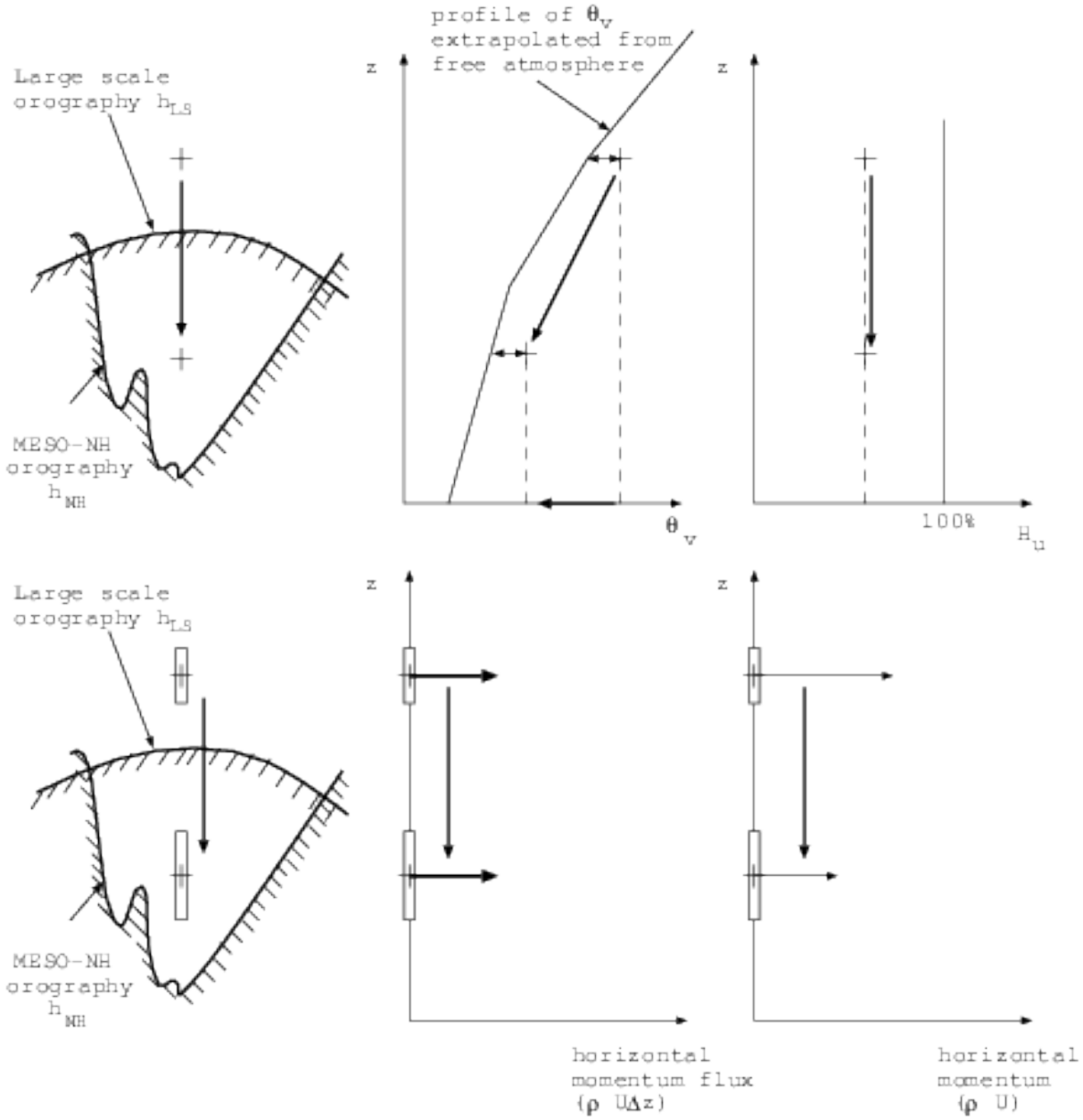

Figure 3.6: Action of the shift on the variables for one point shifted down

The current version of the program conserves

- the difference between θ_v (virtual potential temperature) and θ_v 'free atmosphere profile'. This profile is the one where the boundary layer has been removed. It is constructed in the following manner, which has been found to work fairly well from polar to Saharian boundary layers:
  1. the boundary layer top is found with an algorithm checking $\partial\theta_v/\partial z$, and comparing it to the gradient between 5000 m of height and the ground.
  2. the θ_v values under this boundary layer top are replaced considering a constant gradient equal to the one between 5000 m of height and the boundary layer top.
- the relative humidity $H_u = 100 * p/e_s(T)/(R_d/R_v/r_v + 1)$
- The difference between pressure and hydrostatic pressure. This quantity is zero per definition when input file is an ALADIN one, but is non-zero for a Meso-NH one. This allows to interpolate in some extent the non-hydrostatic effects.
- the horizontal mass flux $\rho Ju, \rho Jv$ in the corresponding grid layer. J is the Jacobian, or volume of the grid box. In practice, since the horizontal grid size is the same for the two grids, it is sufficient to conserve the product of ρu and ρv by the vertical grid size.
- the vertical velocity w. However, it is modified in the upper quarter of atmosphere to obtain a zero value at model top. This will not produce a correct value near the ground (because of new orography). The aim of this is to construct a smooth vertical velocity field for w_{LS}. The initial field w will be produced from this guess by the pressure solver.

Therefore there is usually cooling, moistening, and wind speed decrease if the point is shifted down (in a valley, see Fig. 3.6), and warming, drying and wind speed increase if the point is shifted up (above a peak or ridge).

3.8 Vertical interpolation

The next step is to perform the vertical interpolation from the shifted grid to the Meso-NH grid. Since the two grids share the same definition of the orography, this is relatively straightforward. Llinear interpolation is used.
The variables subject to interpolation are θ_v, H_u, ρu, ρv, w and the difference between pressure and hydrostatic pressure. They are interpolated to the mass points of the Meso-NH grid. Hydrostatism is recomputed from model top, and pressure is deduced afterwards.
Then, r_v is recovered iteratively from θ_v and H_u, and θ from θ_v and r_v by:

$$\theta = \theta_v \frac{1 + r_v}{1 + \frac{R_v}{R_d} r_v} \tag{3.11}$$

Finally, the wind components on the Arakawa C-grid are written as

$$(\rho u) = \overline{(\rho u)}^x \tag{3.12}$$

$$(\rho v) = \overline{(\rho v)}^y \tag{3.13}$$

The fields are now correctly localized on the final Meso-NH grid.

3.9 Reference state

The reference state is computed on the reference grid, as the horizontal average of the actual state. First, $\theta_{v\,ref}$ and $r_{v\,ref}$ are computed as a mean value at constant altitude of the θ_v and r_v field, after interpolation to the reference grid.
Π^{top}_{ref} is computed as the horizontal average of $\Pi^{top}(x,y)$. Then, the hydrostatic relation for the reference state is integrated from top to bottom to compute Π_{ref}.

$$d\Pi_{ref} = -\frac{g}{C_{pd}\theta_{v\,ref}}dz \tag{3.14}$$

Finally, the density of dry air for the reference state is retrieved

$$\rho_{d\,ref} = \frac{P_{00}(\Pi_{ref})^{R_d/C_{pd}-1}}{R_d\theta_{v\,ref}(1+r_{v\,ref})} \tag{3.15}$$

3.10 Computation of the total dry air mass

The total dry air mass within the domain of integration of the model is needed to resolve accurately the pressure problem (see Chapter 2). First, Π is computed by integration of the exact hydrostatic relation

$$d\Pi = -\frac{g}{C_{pd}\theta_v}dz \tag{3.16}$$

from the top ($\Pi^{top}(x,y)$) to the bottom of the integration domain. Then, ρ_d is computed as

$$\rho_d = \frac{P_{00}(\Pi)^{R_d/C_{pd}-1}}{R_d\theta_v(1+r_v)} \tag{3.17}$$

The total dry mass is deduced

$$\mathcal{M}_d = \int\int\int_V \rho_d dV \tag{3.18}$$

3.11 Anelastic constraint

The final step is to enforce the anelastic constraint. The first guess velocity field $\boldsymbol{U}_{fg}$ = (u, v, w) does not verify the lower boundary condition. It also does not satisfy the anelastic constraint, with the reference dry air density. Those two deficiencies are corrected by use of the subroutine ANEL_BALANCE (see previous chapter for a description). The input field for this routine is $\rho_d\boldsymbol{U}_{fg}$, and the output field, $\rho_{d\,ref}\boldsymbol{U}$, satisfies all necessary constraints to start an integration.

Chapter 4

Bogusing for Cyclones

Contents

4.1 Introduction

Mature tropical cyclones are very intense atmospheric disturbances with typical horizontal extent of several hundred to a thousand kilometers, occurring over the most earth's tropical oceanic regions. Wind, storm surges and inland flooding generally associated with tropical cyclones cause, every year, losing of human lives and major material damages in many countries of the tropical belt. Dedicated airborne missions performed over the Atlantic using Doppler radars, but also generally coastal Doppler measurements can permit to deduce kinematic and thermodynamic structure of the vortex.

Meanwhile, since early of 70's, tropical cyclone modeling significantly improved with using of sophisticated parameterization schemes of convection, microphysics, turbulence, surface fluxes,... However, one major drawback of many numerical studies of tropical cyclone is the fact that the initial vortex, usually obtained from global analyses, is often ill-defined, too weak, and sometimes misplaced, leading to subsequent simulation of storm track, structure, and intensity.

The following approach is the one proposed by Nuissier et al. (2005) is which airborne Doppler radar data are used to define a 'specified vortex' for Meso-NH model initialization.

4.2 Method

4.2.1 Removal of the analyzed vortex

To incorporate a hurricane-like vortex with realistic size, depth, and intensity in the Meso-NH initial conditions, it is first necessary to remove the weak vortex analyzed by global models. For this purpose, the scheme proposed by Kurihara et al. (1993 (hereafter KBR93), 1995) is applied. It consists of using appropriate numerical filters to extract the vortex from the large-scale analysis and adding a vortex specified from observations. This can be written symbolically as:

$$[h_i] = [h] - [h_{av}] + [h_s] \tag{4.1}$$

where $[h_i]$ is the initial field (that means zonal and meridian wind, thermal field and optionally the pressure field), $[h]$ is the global analysis, $[h_{av}]$ is the analyzed vortex and $[h_s]$ is the specified vortex.

A low-pass filter with an exponential weighting function, following Barnes (1964), is first applied to the modified large-scale analysis field [h] over the outermost Meso-NH domain to remove features with wavelengths smaller than about 1200 km, the characteristic dimension of the analyzed vortex. The filtering radius is defined precisely by the condition $R_{filt} = \min(R_{Filt}^{User}; 1.25 \times R_{Filt}^{Calculated})$ where R_{Filt}^{User} is the maximal filtering radius giving by the user and $R_{Filt}^{Calculated}$ the calculated filtering radius following the condition ($[V_T < 6\,\mathrm{m.s^{-1}}$ and $\partial V_T/\partial r < 4.10^{-6}\,\mathrm{s^{-1}}]$ or $V_T < 3\,\mathrm{m.s^{-1}}$), where V_T is the tangential wind. Using the same terminology as KBR93, this produces the basic field $[h_b]$, which is subtracted from $[h]$ to obtain the total disturbance field $[h_d]$:

$$[h] - [h_b] = [h_d] = [h_{av}] + [h_{nh}] \tag{4.2}$$

where $[h_{nh}]$ is the none-hurricane disturbance.

The next step consists of extracting $[h_{av}]$ from $[h_d]$. This is done using the same cylindrical filter as that proposed by KBR93:

$$h_{av}(r,\theta) = h_d(r,\theta) - [h_d(r_0,\theta)E(r) + h_d(r_0)(1 - E(r))] \tag{4.3}$$

where r and θ are the radius and the azimuth relative to the center of the analyzed vortex, r_0 is the radius at which the value of weighting function E(r)=1, and $h_d(r_0)$ is the mean value of $h_d(r,\theta)$ for $r = r_0$ and $0 \leq \theta < 2\pi$. The function E(r) (see Eq. (3.8) and Fig. 2b in KBR93) is an empirically determined exponential equation which increases smoothly from 0 at $r = 0$ to 1 at $r = r_0$, with a smooth transition between the inner (i.e. hurricane component for $r < r_0$) and the outer regions (i.e. non-hurricane component for $r > r_0$).

4.2.2 A 'specified vortex' derived from airborne Doppler radar observations

After the analyzed vortex has been removed, the resulting environmental fields are used as new large-scale conditions, and interpolated over the other innermost Meso-NH domains. A symmetrical radar-derived vortex deduced from Doppler radar observations is then added to this modified large-scale field in every Meso-NH domains. This method is referred to as the 'Radar Vortex Conditioning' (RVC).

The wave number-0 component (symmetrical part) of the tangential wind is first deduced from the Extended Velocity-Track Display (EVTD) or Ground-Based Velocity-Track Display (GB-VTD) analysis (Roux and Marks 1996, Roux et al. 2004). Although the EVTD-derived velocities bring

valuable information on the storm dynamic structure, they do not cover a large enough domain to properly define the specified vortex. Hence, an analytic model is used to describe the radial and vertical distribution of the tangential wind over a larger domain. The analytic wind $V_T(r,z)$, where z is altitude, is defined through the formulation proposed by Holland (1980), as:

$$V_T(r,z) = \sqrt{V_{Tmax}^2(z) \times \frac{\exp\left\{1 - 1/[r/RMW(z)]^{B(z)}\right\}}{[r/RMW(z)]^{B(z)}} + \left[\frac{fr}{2}\right]^2} - \left|\frac{fr}{2}\right| \tag{4.4}$$

where $V_{Tmax}(z)$ is the maximum wind, f is the Coriolis parameter, $RMW(z)$ is the radius of maximum wind, and $B(z)$ is a scaling parameter for the radial variation of the wind. We can notice that the tangential wind is not an axisymmetric field because of the Coriolis parameter. In order to avoid spurious variations of V_{Tmax}, RMW and B between the different levels, they suppose to obey the following relations with respect to z:

$$V_{Tmax}(z) = V_{Tmax}(z=0)\left[1 - \frac{z}{z_{max}}\right]^c \tag{4.5}$$

$$RMW(z) = RMW_0 \times \left[1 + \rho_z \times \frac{z}{z_{max}} + \rho_{zz} \times \left[\frac{z}{z_{max}}\right]^2\right] \tag{4.6}$$

$$B(z) = B_0 \times \left[1 + \beta_z \times \frac{z}{z_{max}} + \beta_{zz} \times \left[\frac{z}{z_{max}}\right]^2\right] \tag{4.7}$$

where B_0, β_z, β_{zz} are fixed values. Once z_{max}, $V_{Tmax}(z)$ and $RMW(z)$ have been determined at each level from the EVTD-derived tangential winds, coefficients $V_{Tmax}(z=0)$ and C in (4.5), RMW_0, ρ_z, ρ_{zz} in (4.6) are deduced from least-squares fits along the vertical. Then, parameters B_0, β_z, β_{zz} in (4.7) are deduced from a least-squares fit of the EVTD-derived winds in the radius-height domain, with the constraint that $B(z)$ must be between 1.0 and 2.5 (Holland 1980).
To create the initial field $[h_i]$ following (4.1), the specific vortex $[h_s]$ is added on a domain $r \leq R_{bog}$ where R_{bog} is defined following the condition $V_T(R_{bog}, z=0) = 0.5\,\mathrm{m.s^{-1}}$ with $R_{bog} > RMW_0$ and where V_T is defined by (4.4) with a fixed value for the Coriolis parameter $f = f_{bog}$ at the center of the bogus.

4.2.3 The thermal-wind balance

As shown by other studies, a numerical model may produce more realistic tropical cyclones when a specified vortex includes wind and sea-level pressure information. Pressure perturbations associated with a tropical cyclone are mainly caused by hydrostatic effects due to the warm anomaly at its center. Hence, the specified vortex to be added to the large-scale analysis must include complementary descriptions of the cyclonic wind and temperature perturbations. Temperature can be deduced from the analytic tangential wind $V_T(r,z)$ in (4.4) through the thermal-wind relation:

$$\frac{\partial}{\partial r}\theta_1(r,z) = \frac{\theta_0(z)}{g}\left[2\frac{V_T(r,Z)}{r} + f\right]\frac{\partial}{\partial \zeta}V_T(r,Z) \tag{4.8}$$

where θ_0(z) is the potential temperature in the environment ($[h_b]$ in 4.2), $\theta_1(r,z)$ is the cyclonic perturbation, f is the Coriolis parameter, g is the acceleration due to gravity, Z is a modified vertical coordinate such that $Z = z \times \langle\theta_0\rangle / \theta_0(z)$, where $\langle\theta_0\rangle$ is the mean value of $\theta_0(z)$. $\theta_1(r,z)$ is obtained from the horizontal integration of (4.8) starting from 0 to the bogus radius R_{bog}.

Figure 4.1 illustrates the RVC methodology for the case of Hurricane Bret on 22-23 August 1999 over the Gulf of Mexico, from the ECMWF large-scale analysis. Fig. 4.1a shows that the ECMWF model, because its coarse horizontal resolution, failed to properly reproduce the mature hurricane, whereas the 'specified' radar vortex highlights wind maximum intensity much stronger and closer to the hurricane center (Fig. 4.1b).

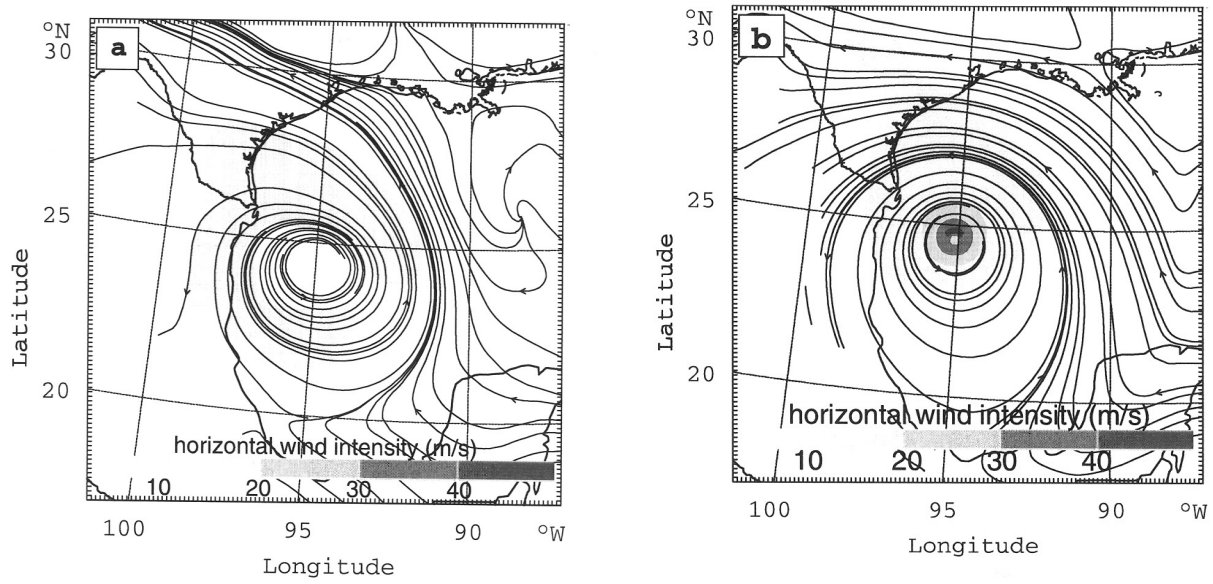

Figure 4.1: Horizontal streamlines at 850 hPa for Hurricane Bret on 22 August 1999 from (a) the ECMWF global analysis at 00 UTC and (b) the inclusion of the airborne Doppler-derived "specified"

4.2.4 The radial circulation

It must be emphasized that the EVTD analysis could permit to retrieve a realistic structure of the secondary circulation (i.e. updraft centered on the radius of maximum wind, inflow (outflow) in the lower (upper) part of troposphere). In numerical models (as in reality) the radial and vertical circulation results from: sensible- and latent-heat fluxes from the ocean surface increasing θ_e in the lowest atmospheric layers; surface friction inducing radial convergence; latent-heat release sustaining vertical motions through thermal buoyancy; and vertical momentum fluxes generating horizontal and vertical pressure perturbation gradients. Including these physical constraints in an analytical formulation of a symmetric secondary circulation would be a very difficult task.
However it is easy to include the effect of surface friction. Indeed according to the Ekman theory, the friction forces due to the surface (ocean or land) induce a radial convergence in the lower layers. The frictional verring (in radian) is given by:

$$\left\{ \begin{array}{rcll} \alpha_{friction}^{Ekman}(lat,z) & = & |z-H_{cl}| \times \sqrt{\frac{|f|}{2K}} & \text{for } z < H_{cl} \\ & = & 0 & \text{for } z \geq H_{cl} \end{array} \right. \tag{4.9}$$

where H_{cl} is the height of the boundary layer and K the Ekman exchange ratio (which is constant). It is therefore a linear function of altitude but independent of the wind and hence the distance from the centre. By cons, it is a function of latitude through the Coriolis parameter. However this theory

leads to severe restrictions on the atmosphere that are not verified. Climatological studies (Gray 1968, 1972) on tropical depressions can highlight a profile of inflow in low levels by friction. Such a climatological profile is characterized by (4.10), whatever the latitude and intensity of the wind (hence the distance from the centre of the system):

$$\begin{cases} \alpha_{friction}^{Clim}(z) & = & 12^\circ & \text{for } 0 \leq z \leq 1000\,\text{m} \\ & = & 3^\circ & \text{for } 1000\,\text{m} < z \leq 2000\,\text{m} \\ & = & 0^\circ & \text{for } 2000\,\text{m} < z \end{cases} \tag{4.10}$$

To include this convergence, the radial wind is calculated following the relation $V_R(r,z) = V_T(r,z) \times \tan \alpha_{friction}(z)$ where $V_T(r,z)$ is obtained by (4.4) and $r \geq RMW$. We can notice that radial wind is nil for $r < RMW$, positive for an inflow and is no axisymmetric field because of the Coriolis parameter in $V_T(r,z)$. The user can choose the values of the friction angle but thought the climatological values are preferable, the default value being nil. For every point (i, j, k), the bogusing wind is:

$$\begin{cases} U_{bog} & = & -V_T \sin\phi - V_R \cos\phi \\ V_{bog} & = & V_T \cos\phi - V_R \sin\phi \end{cases} \tag{4.11}$$

where, for a vertical model level k, ϕ is the projection angle on the meridian axis of the vector $\overrightarrow{I_{bog}M}$, defined by the bogus center I_{bog} and the considered point $M_{(i,j)}$.

4.3 References

Barnes, S. L., 1964: A technique for maximizing details in numerical weather map analysis. *J. Appl. Meteor.*, **3**, 396-409.

Gray, W. M., 1968: Global view of the origin of tropical disturbances and storms. *Mon. Weather Rev.*, **96**, 669-700.

Gray, W. M., 1972: Diagnostic study of the planetary boundary layer over the oceans. *Technical Report 179*, Colorado State University.

Holland, G. J., 1980: An analytic model of the wind and pressure profile in hurricanes. *Mon. Weather Rev.*, **108**, 1212-1218.

Kurihara, Y., M. A. Bender, and R. J. Ross, 1993: An initialization scheme of hurricane models by vortex specification. *Mon. Weather Rev.*, **121**, 2030-2045.

Kurihara, Y., M. A. Bender, R. E. Tuleya, and R. J. Ross, 1995: Improvements in the GFDL hurricane prediction system. *Mon. Weather Rev.*, **123**, 2791-2801.

Nuissier, O., R. F. Rogers, and F. Roux, 2005: A numerical simulation of Hurricane Bret on 22-23 August 1999 initialized with airborne Doppler radar and dropsonde data. *Quart. J. Roy. Meteor. Soc.*, **131**, 155-194.

Roux, F. and F. D. Marks Jr, 1996: Extended Velocity Track Display (EVTD): An improved processing method for Doppler radar observations of tropical cyclones. *J. Atmos. Oceanic. Technol.*, **13**, 875-899.

Roux, F., F. Chane-Ming, A. Lasserre-Bigorry, and O. Nuissier, 2004: Structure and evolution of intense tropical cyclone Dina near la Réunion on 22 January 2002: GB-EVTD analysis of single Doppler radar observations. *J. Atmos. Oceanic. Technol.*, **21**, 1501-1518.

Chapter 5

Physiographic Data

Contents

type of data	resolution	area	file name
surface cover type	1km	global	ecoclimats_v1
orography	1km	global	gtopo30
clay fraction	10km	global	clay_fao
sand fraction	10km	global	sand_fao

Table 5.1: Default data files.

5.1 Introduction

As shown in many studies, a good representation of land surface characteristics is often necessary for numerical models to reproduce realistically certain meteorological events and climatological patterns. For example, particular atmospheric phenomena such as mesoscale waves, typical precipitation patterns, blocking of synoptic systems, and cyclogenesis, can be generated or induced by the topography, thereby indicating the need to use realistic and high-resolution two-dimensional fields in numerical models to represent this surface feature. Similarly, the land-water mask, the soil-vegetation characteristics, and the urbanized area locations are required for the calculation of surface fluxes of heat, moisture, and momentum over continental and oceanic surfaces. Other surface fields, like the albedo and emissivity, have direct effects on the radiation balance at the surface and in the atmosphere.
For the Meso-NH atmospheric model, the determination of the two-dimensional surface fields reveals to be particularly crucial and difficult. Crucial because many of the scientific purposes of this model are related to the examination of mesoscale circulations generated by discontinuities in the surface characteristics (e.g., mountain waves, sea and land breezes, urban heat island, meso-γ fluxes heterogeneities); and difficult since this model can be run at horizontal resolutions ranging from the micro-scale to the meso-α scales, thereby making the automatic generation of surface fields bewildering. Nevertheless, it is the aim of this part of the Meso-NH atmospheric modelling system to produce an MNH file containing all the surface fields necessary for an integration of the model. Such a file is called a PGD file (for 'PhysioGraphic Data file'). This is done by a program called PREP_PGD, which averages (or interpolates) the geographic data onto the MESONH grid. The averaging is arithmetic, except for some fields, such as heat capacities and stomatal resistances (where it is harmonic), or for roughness lengths.

Since many users will want to use their own physiographic data sources (especially for very high resolution runs, some hundreds of meters or less), we have designed a system which allows easy interfacing with the model. This is based on "data files" having a very general and simple format. How to use such data files is explained in the MESO-NH book3.
However, for those users that are not preoccupied by these problems, we also provide default data files. These have a very good resolution, of the order of 30 seconds (approximately 1 km), they are global, and thus assure the MNH users that correct surface characteristics will be considered in their simulation, regardless of the position of the model grid on the globe. Over Europe, a surface cover type file with finer resolution (250m) is available.
The default information comes from 4 distinct data files (see tabledataPGD).
All the physiographic data necessary to the different parameterizations of the MESO-NH model are recovered from these data. The next section presents the surface cover type data. The following section will present the fields computed from the surface cover type. The next one the fields computed with the orographic data.

5.2 The surface cover types

The most important data is the cover type. A surface cover type is the type of landscape that is present at a certain location: sea, river, forest, town, grassland, crops, desert... Idealy, the more the cover types are, the more it is possible to refine the description of each location. The default data file contains 250 cover types. This is fine enough (as will be presented in next section) to derive reasonable vegetation parameters all around the world. Here is explained how this file was built:

5.2.1 On the world, except Europe

1. the coastline, lakes and river paths (finer data, resolution 1km) come from the Digital Chart of the World (DCW) data.

2. 15 main cover types come from the University of Maryland data (Hansen et al. 2000) derived from satellite NOAA/AVHRR. The two last cover types come from the IGBP-DIS data set (Belward 1996). The resolution of these two datasets is 1km. However, we can consider that the real resolution is about a few kilometers. These types are:

   (a) evergreen needleleaf forest
   (b) evergreen broadleaf forest
   (c) deciduous needleleaf forest
   (d) deciduous broadleaf forest
   (e) mixed forest
   (f) woodland
   (g) wooded grassland
   (h) closed shrubland
   (i) open shrubland
   (j) grassland
   (k) cropland
   (l) bare soil
   (m) urbanized areas
   (n) permanent snow and ice
   (o) wetlands

3. The problem is that this classification does take into account only the most general pattern of the cover. In reality, an open shrubland in polar regions (tundra) and in tropical aeras (savana) will have a very different vegetative behaviour. The same stands for all these main types. Therefore, a map of climates of the world derived from Koeppe and De Long (1998) was used to add a discrimination between these cover types. 16 climates were used:

   (a) dry summer subtropical
   (b) tropical desert
   (c) semiarid tropical

(d) wet and dry tropical

(e) wet equatorial

(f) trade wind littoral

(g) humid subtropical

(h) semiarid continental

(i) intermediate desert

(j) moderate polar

(k) cool marine

(l) polar

(m) cool littoral

(n) humid continental

(o) extreme subpolar

(p) marine subpolar

4. The combination of the 15 cover types with the 16 climates for the six continents (both for northern and southern hemisphere parts for Africa, South-america and Oceania) led to a very important number of possible 'ecosystems'. Some of them occupy a very small area on the earth, and are not representatives. Others, even in different climates or continents have a very similar behaviour. In order to discriminate the representative cover-climate ecosystems, the 1km NDVI composites from NOAA/AVHRR from April 1992 to March 1993 (Eidenshink and Faudeen 1994) were used. Aggregation between different ecosystems into one representative ecosystem was performed according to the following rules:

   - an ecosystem with one cover type can not be aggregated with one other ecosystem with another cover type (e.g. closed shrubland will not be aggregated with open shrubland). This respects the main cover types above. Exception: a forest could be aggregated with another forest, leading either to a forest with one of their type (needleleaf or broadleaf, evergreen or deciduous), or to a mixed forest.
   - the aggregation was performed with priority between climates on one continent. This was perfomed comparing the NDVI annual profiles (minimum, maximum, shape of the profile). When more than one month seperates the minimum (or the maximum) of two profiles, they were considered to be representative of two different vegetations, and were not aggregated. The ecosystems in the 'wet equatorial' climate must be the same on the two sides of the equator.
   - if two NDVI profiles for two ecosystems of the same cover type are found on several continents, they could also be aggregated.

   Finally, this procedure lead to 125 representative cover types on the world (except Europe). They are really representative of one vegetation behaviour, allowing to derive vegetation parameters for each of them (leaf are index, fraction of forest, roughness,...).

5.2.2 On Europe, for the 1km map

The same procedure was used over Europe, but with initial data at a better resolution:

1. where available, the coastline is derived from the CORINE land cover data set (resolution 250m), averaged at 1km.
2. the cover types are issued from CORINE land cover when available. When not available, they come from the PELCOM data set (Mucher, 2000). The main goal of PELCOM project, which was an European project, was to obtain a 1km pan-european land cover database from NOAA/AVHRR.
3. the climate map is derived on Europe from the FIRS project.
4. this leads to about 100 ecosystems on Europe

5.3 Fields deduced from the surface cover types

5.3.1 Sea, inland water, town and artificial surfaces, natural and cultivated landscape

field	notation	unit
fraction of sea	f_{sea}	-
fraction of artificial areas	f_{town}	-
fraction of inland water	f_{water}	-
fraction of natural and cultivated areas	f_{nature}	-

Table 5.2: Main surface parameters.

These four surface types are the most important fields deduced from the cover types. They define the partition of the grid mesh between four very different surfaces. During the MESO-NH run, a particular surface scheme will be used for each of them to compute the energy fluxes towards the atmosphere. Then, the four fluxes will be averaged according to the surface occupied by each surface, in order to retrieve the global energy fluxes to the atmosphere.
Default values for these four fields are prescribed for each of the representative ecosystems: for example, natural surface fraction is 1 for forest, but only 0.3 for urban areas (garden), while the other 0.7 are for artificial areas. See appendix for details.

5.3.2 Artificial parameters

field	notation	unit
geometric parameters		
fractional artificial area occupied by buildings	a_{bld}	-
fractional artificial area occupied by roads	$1 - a_{bld}$	-
building height	h	m
building aspect ratio	h/l	-
canyon aspect ratio	h/w	-
dynamic roughness length for the building/canyon system	$z_{0_{town}}$	m
radiative parameters		
roof, road and wall albedos	α_R, α_r, α_w	-
roof, road and wall emissivities	ϵ_R, ϵ_r, ϵ_w	-
thermal parameters		
thickness of the k^{th} roof, road or wall layer	d_{R_k}, d_{r_k}, d_{w_k}	m
thermal conductivity of the k^{th} roof, road or wall layer	λ_{R_k}, λ_{r_k}, λ_{w_k}	W m^{-1} K^{-1}
heat capacity of the k^{th} roof, road or wall layer	C_{R_k}, C_{r_k}, C_{w_k}	J m^{-3} K^{-1}

Table 5.3: Parameters of the TEB scheme. *Note that some surfaces between the buildings, such as gardens or parks for example, are* **not** *treated by the TEB model, but modify the canyon width,* w.

For each of the cover types partially or totally covered by artificial areas (typically urban areas), some parameters describing the surface are needed. These parameters will be used in the 'Town Energy Budget' model (Masson 2000).

5.3.3 Water parameters

field	notation	value
water near-infra-red albedo	$\alpha_{nir_{wat}}$	0.20
water visible albedo	$\alpha_{vis_{wat}}$	0.07
water emissivity	ϵ_{wat}	0.98
sea ice near-infra-red albedo	$\alpha_{nir_{ice}}$	0.85
sea ice visible albedo	$\alpha_{vis_{ice}}$	0.85
sea ice emissivity	ϵ_{ice}	1.

Table 5.4: Water and Sea ice parameters

At the time being, the physiographic fields (albedos and emissivity) for water are uniform.
Occurence of sea ice is detected using the Sea Surface Temperature (coming from the meteorological analyses). If SST is below two degrees below 0° (273.15K), then the sea surface is assumed to be frozen. Its radiative parameters correspond to those of fresh snow.

5.3.4 Main natural landscape parameters parameters

field	notation	unit
fraction of vegetation type		-
trees	f_{trees}	
grassland	f_{grass}	
C3 type crops	f_{C3}	
C4 type crops	f_{C4}	
bare soil (smooth)	f_{bare}	
rocks	f_{rocks}	
permanent snow	f_{snow}	
Leaf Area Index (monthly)	LAI	m^2/m^2
height of trees	h	m
root depth	d_2	m
soil depth	d_3	m

Table 5.5: Main ISBA parameters.

When a representative ecosystem contains some vegetated or bare soil part (this is the most common case, the only exception being for sea or inland water types), surface parameters are needed to describe both the vegetation and its horizontal extension.
Some parameters are prescribed for each ecosystem.

- The fractions of each type of vegetation are estimated from the 15 main cover types (before climatic treatment). Small variations are allowed for ecosystems coming from the same main cover type. For example, some wooded grassland contains more bare soil than some other ones, and then less trees or grass.

- The Leaf Area Index (LAI) is the surface of leaves per surface of ground (m^2/m^2). It describes the amount of **green** vegetation over the area. A monthly evolution of the LAI is necessary, to describe the annual cycle of the vegetation. For the default data files, LAI is deduced from measured NDVI profiles, with consideration of the type of vegetation (there is less LAI over wooded grassland than over forest, even if NDVI is close). A LAI profile is defined for each representative ecosystem.

  However, if a user wants to use directly his (or her) LAI data, it is possible to include it during the PREP_PGD step, and this LAI will be used during the MESONH run.

- The height of trees is defined for the representative ecosystems containing trees. It is used to compute the roughness length of the vegetation.

- The root depth d_2 defines the area within the soil reached by the vegetation roots. The transpiration of the vegetation takes water in the soil by these roots.

- The total soil depth d_3 is not strictly a vegetation parameter. This is an approximation to use the ecosystems to define this depth, but it is legitimated by the fact that in the ISBA scheme, this is the soil area which is in interaction with the root layer above (water goes up by capillarity if transpiration occurs). Therefore, it depends of the type of the vegetation above.

5.3.5 Other natural landscape parameters parameters

field	notation	unit
vegetation fraction (green veg. + dead biomass)	veg	-
vegetation roughness length for momentum	$z_{0_{veg}}$	m
vegetation roughness length for heat	$z_{0h\,veg}$	m
emissivity of the ecosystem	ϵ_{eco}	-
near-infra-red albedo of the vegetation (only)	$\alpha_{nir_{veg}}$	-
visible albedo of the vegetation (only)	$\alpha_{vis_{veg}}$	-
minimum stomatal resistance	$r_{s_{min}}$	sm^{-1}
coefficient for the calculation of the stomatal resistance	γ	-
maximum solar radiation usable in photosynthesis	rgl	Wm^{-2}
mesophyl conductance	gm	ms^{-1}
biomass LAI ratio	B/lai	kgm^{-2}
e-folding time for senescence	e_{fold}	days
$2\sqrt{\frac{\pi/\tau}{C_{veg}\lambda_{veg}}}$	C_v	Km^2J^{-1}

Table 5.6: other ISBA parameters.

The other ISBA scheme parameters are computed from the parameters described in previous section. If a user wants to use its own data for some of these parameters, it is still possible.
Vegetation type, Leaf area index and height of vegetation (for trees) are used in these computations. Because the Lai is representative of the entire surface, it is not used directly, but is re-scaled on the potentially vegetated surface:
$\hat{lai}$ is the leaf area index corresponding to the area occupied by trees, grassland, and C3 and C4

crops, excluding bare land, rocks and snow types: $\hat{lai} = \frac{lai}{f_{tree}+f_{grass}+f_{C3}+f_{C4}}$. Therefore, $\hat{lai}$ is greater than the area averaged lai (lai is zero on bare surfaces).

vegetation fraction

veg =	$1 - e^{-0.6\hat{lai}}$	for C3 cultures, C4 cultures
veg =	0.95	for grassland
veg =	$1 - e^{-0.5\hat{lai}}$	for trees
veg =	0.	for bare soil, snow and rocks

When averaging is needed, it is performed arithmetically

roughness length for momentum

The height of the vegetation is computed as:

h_{veg} =	min $(1., h_{allen})$	for C3 cultures
h_{veg} =	min $(2.5, h_{allen})$	for C4 cultures
h_{veg} =	h	for trees
h_{veg} =	$\hat{lai}/6$	for grassland
h_{veg} =	0.01 m	for bare soil and snow
h_{veg} =	1. m	for rocks

where $h_{allen} = e^{(\hat{lai}-3.5)/1.3}$
The roughness length is deduced: $z_{0_{veg}} = 0.13 h_{veg}$
When averaging is needed, it is performed according to the $1/\ln^2(\frac{z_{0veg}}{10})$ quantities.

roughness length for heat

$z_{0h\,veg}$ is equal to one $10^{\,th}$ of $z_{0\,veg}$

emissivity

Emissivity is equal to 0.99 on the vegetated part (veg), to 0.96 on bare soil and rocks, and to 1. on snow. Averaging is linear.

other vegetation parameters

Other vegetation parameters are computed from the vegetation types. The 'bare soil', 'rocks' and 'snow' vegetation types are not pertinent. When averaging is needed, it is performed linearly, except for the C_v parameter, where it is harmonic.

	$\alpha_{nir_{veg}}$	$\alpha_{vis_{veg}}$	$r_{s_{min}}$	γ	rgl	gm	B/lai	e_{fold}	C_v
trees	.15	.05	150	.04	30	.001	.25	365.	1. 10^{-5}
C3 crops	.30	.10	40	0.	100	.003	.06	60.	2. 10^{-5}
C4 crops	.30	.10	40	0.	100	.003	.06	60.	2. 10^{-5}
grassland	.30	.10	40	0.	100	.020	.36	90.	2. 10^{-5}

5.4 Soil characteristics

5.4.1 Composition of the soil

field	notation	unit
clay fraction	f_{clay}	-
sand fraction	f_{sand}	-

Table 5.7: composition of the soil

The soil is supposed to be of uniform compostion over its total depth (but it can vary horizontally). It is defined by its sand and clay fractions. These come from the FAO database.

5.4.2 Color of the soil

field	notation	unit
near-infra-red albedo for dry bare soil	$\alpha_{nir_{dry}}$	-
visible albedo for dry bare soil	$\alpha_{vis_{dry}}$	-
near-infra-red albedo for wet bare soil	$\alpha_{nir_{wet}}$	-
visible albedo for wet bare soil	$\alpha_{vis_{wet}}$	-

Table 5.8: composition of the soil

At the time being, there is no soil color data incorporated in MESO-NH. An estimation of the **dry** bare soil albedo is computed from the sand fraction, using linear formulae:

$$\alpha_{vis_{dry}} = 0.05 + 0.30\, f_{sand}$$

$$\alpha_{nir_{dry}} = 0.15 + 0.30\, f_{sand}$$

If the soil is wet, it is darker. This happens when soil water content reaches the field capacity (capilarity and gravity are in equilibrium). The albedos for wet soil are estimated as:

$$\alpha_{vis_{wet}} = \frac{1}{2}\, \alpha_{vis_{dry}}$$

$$\alpha_{nir_{wet}} = \alpha_{nir_{dry}} - \frac{1}{2}\, \alpha_{vis_{dry}}$$

5.5 Orography

field	notation	unit
mean orography	z_{smean}	m
envelop orography	z_{senv}	m
silhouette orography	z_{ssil}	m

Table 5.9: orography

Three types of orography can be computed by **PREP_PGD**: mean, envelop or silhouette orography. Note that orography is not computed on seas, where it is automatically set to zero.

5.5.1 Mean orography

This orography is simply the averaged of the subgrid-scale-orography in each grid mesh.

5.5.2 Envelope orography

This envelope orography is computed as the mean orography in each grid mesh z_{smean} plus a contribution from the smaller scales, proportional to the subgrid scale orography standard deviation μ_{z_s}. This reads

$$z_{senv} = z_{smean} + XENV * \mu_{z_s}, \tag{5.1}$$

where XENV is a parameter of the namelist. For XENV=0, one obtains the mean orography.

5.5.3 Silhouette orography

The silhouette orography is computed as shown on figure 5.1, from the maximum relief silhouette one could see in the grid mesh, looking in x and y directions. The 'resolution of the eye' is given by the parameter XSIL, expressed in meters (also see book3):

- XSIL = grid mesh width :
  one obtains the maximum relief in the mesh.
- XSIL = resolution of input data :
  one obtains the typical silhouette orography.
- XSIL $\rightarrow$ 0 :
  one obtains the mean orography, since all the points will be seen in the silhouettes[1].

[1]except if input data is exactly located following x and y directions; it is the case in Mercator projection without rotation with input data on a regular latitude-longitude grid. In this case, one obtains again the typical silhouette orography

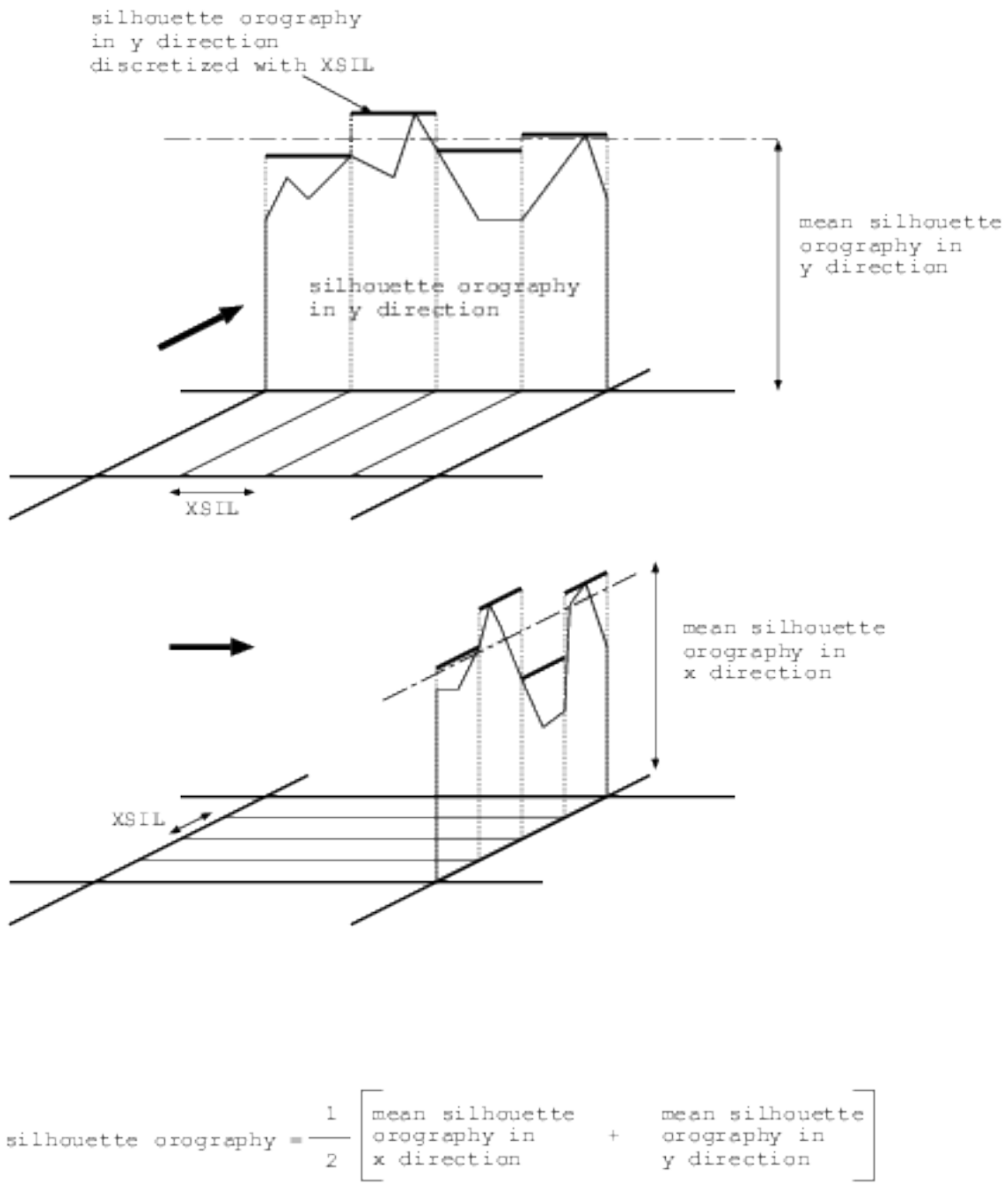

Figure 5.1: Computation of silhouette orography in one grid mesh

5.6 Subgrid-scale orographic parameters

5.6.1 Roughness length for momentum

field	notation	unit
obstacle front area (A) over mesh surface (S) in each direction	$\sum A_{i+}/S, \sum A_{i-}/S$ $\sum A_{j+}/S, \sum A_{j-}/S$	-
characteristic heights of obstacles encountered in each direction	h_{i+}, h_{i-}, h_{j+}, h_{j-}	m
subgrid-scale-orography dynamical roughness lengths in each direction	$z_{0eff_{i+}}$, $z_{0eff_{i-}}$, $z_{0eff_{j+}}$, $z_{0eff_{j-}}$	m
subgrid-scale-orography dynamical roughness length	z_{0rel}	m

Table 5.10: parameters for roughness lengths computations

Roughness lenghts are computed along each model main axis (x and y) and in both directions, leading then to four roughness lengths. They are computed according to Mason (1991), as in Georgelin *et al* (1994), in each direction:

$$\frac{1}{ln^2\left(\frac{h_{i+}}{2z_{0eff_{i+}}}\right)} = \frac{0.5C_D\sum A_{i+}}{Sk^2} + \frac{1}{ln^2\left(\frac{h_{i+}}{2z_{0veg}}\right)} \tag{5.2}$$

where C_D is a drag constant near unity, depending on obstacle shape (equal to 0.8), and k is the Von Karman constant, 0.4.
Note that the roughness lengths are computed both from subgrid-scale orographic parameters and from vegetation roughness length for momentum. The uni-directional roughness length z_{0rel} is defined as the mean of the four directional roughness lengths.

5.6.2 Subgrid-scale orography structure

field	notation	unit
subgrid-scale-orography standard deviation	μ_{z_s}	m
subgrid-scale-orography anisotropy	γ_{z_s}	-
direction of small axis of subgrid-scale-orography according to x axis	θ_{z_s}	$^\circ$
subgrid-scale-orography characteristic slope	σ_{z_s}	-

Table 5.11: Subgrid-scale orography structure parameters

The computations of these parameters is performed as in Lott and Miller 1997. One uses the topographic correlation tensor, defined according to the directions i and j of the model domain axes on the conformal plane (and not the input data axes, since data is not necessary on a regular grid). As for the case of the silhouette orography, a parameter is used to define the subgrid sampling of the data, in order to compute the subgrid gradients (also see book3). This allows to use any orographic data set directly in PREP_PGD, without any necessary prior computation.

The tensor is diagonalized to find the directions of the principal axes and the degree of anisotropy. If

$$K = \frac{1}{2}\left\{\overline{\left(\frac{\partial h}{\partial x}\right)^2} + \overline{\left(\frac{\partial h}{\partial y}\right)^2}\right\} \qquad L = \frac{1}{2}\left\{\overline{\left(\frac{\partial h}{\partial x}\right)^2} - \overline{\left(\frac{\partial h}{\partial y}\right)^2}\right\} \qquad M = \overline{\frac{\partial h}{\partial x}\frac{\partial h}{\partial y}}$$

Then the angle of the main axis according to i axis is:

$$\begin{array}{lll} \theta_{z_s} = & \frac{\pi}{4} & \text{if } L = 0 \\ \theta_{z_s} = & \frac{1}{2}\arctan(M/L) & \text{if } L > 0 \\ \theta_{z_s} = & \frac{1}{2}\arctan(M/L) \quad +\frac{\pi}{2} & \text{if } L < 0 \end{array}$$

The slope parameter is defined as:

$$\sigma_{z_s}^2 = K + \sqrt{L^2 + M^2}$$

The anisotropy is given by:

$$\begin{array}{lll} \gamma_{z_s}^2 = & 1 & \text{if } \sigma_{z_s} = 0 \\ \gamma_{z_s}^2 = & \frac{K - \sqrt{L^2+M^2}}{K + \sqrt{L^2+M^2}} & \text{if } \sigma_{z_s} > 0 \end{array}$$

5.7 Appendix: default parameters for the ecosystems

5.8 References

Belward, A.S., ed., 1996, The IGBP-DIS global 1 km land cover data set (DISCover)-proposal and implementation plans: IGBP-DIS Working Paper No. 13, Toulouse, France, 61 pp.

Eidenshink, J.C. and Faundeen, J.L., 1994: The 1 km AVHRR global land data set-first stages in implementation. *Int. J. Remote Sensing*, **15**, 443-3,462.

Georgelin, M. and E. Richard and M. Petitdidier and A. Druilhet, 1994: Impact of subgrid scale orography parameterization on the simulation of orographic flows. *Mon. Wea. Rev.*, **122**, 1509-1522.

Hansen, M.C., DeFries, R.S., Townshend, J.R.G., and Sohlberg, R., 2000: Global land cover classification at 1km spatial resolution using a classification tree approach. *Int. J. Remote Sensing*, **21**, 1331-1364.

Koeppe, C. E. and De Long G. C., 1998: Weather and Climate. Mc Graw-Hill book company.

Lott, F. and M. J. Miller, 1997: A new subgrid-scale orographic drag parameterization: its formulation and testing. *Quart. J. Roy. Meteor. Soc.*, **123**, 101-127.

Mason, P. J., 1991: Boundary-layer parameterization in heterogeneous terrain. *Workshop Proc. on Fine Scale Modelling and the Development of Parameterizations Schemes, ECMWF*, 275-288.

Masson, 2000: A physically-based scheme for the urban energy budget in atmospheric models. *Bound. Layer. Meteor.*, **94**, 357-397.

Chapter 6

Surface Processes Scheme

Contents

Since the **Meso-NH** Masdev4-6 version, the surface schemes were externalized in the so-called **SURFEX** scheme. In absence of scientific documentation associated with SURFEX, the documentation of the surface schemes, as it was in the Meso-NH Masdev4-3 version is given below, as the principles of most of the surface schemes remain the same.

6.1 Introduction

By providing more realistic lower boundary conditions, land surface schemes can help to improve the numerical simulation of the atmosphere. The surface and the atmosphere interact via energy fluxes applied at the base of the atmospheric numerical model. The fluxes provided to the atmospheric model are the momentum flux, turbulent sensible and latent heat fluxes, the upward radiative fluxes, and, as an option, the CO2 flux.
The MESO-NH grid box is partitioned in 4 main surface types: sea, inland water, towns (artificial areas only), natural and cultivated areas (including gardens and town parks). In order to keep the subgrid surface type information, an appropriate surface scheme is used to compute the fluxes between each of the surfaces and the atmosphere (assumed identical for all the sub-components). Then, the averaging of the 4 fluxes gives the flux received by the atmospheric part of MESO-NH.

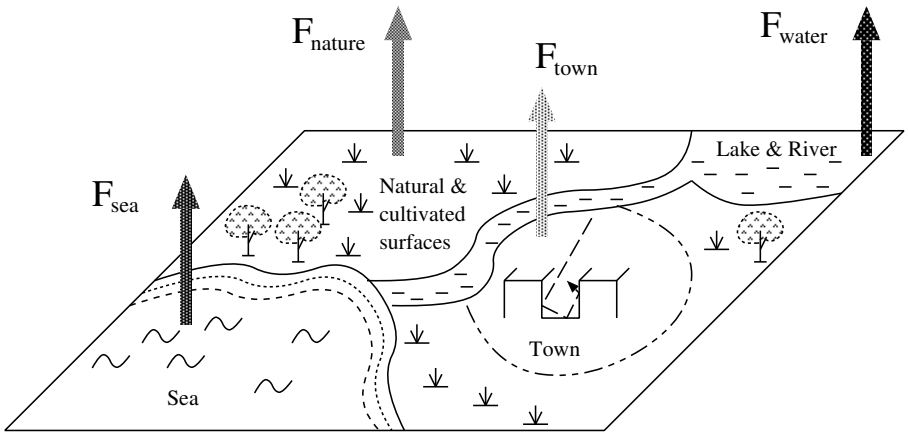

Figure 6.1: Partitioning of the MESO-NH grid box, and corresponding turbulent fluxes. F stands either for M (momentum flux), H (sensible heat flux), LE (latent heat flux), $S^{\uparrow}$ (the reflected solar radiation) or $L^{\uparrow}$ (the upward longwave radiation).

$$
\begin{array}{lcllllll}
M & = & M_{sea} & + & M_{water} & + & M_{town} & + & M_{nature} \\
H & = & H_{sea} & + & H_{water} & + & H_{town} & + & H_{nature} \\
LE & = & LE_{sea} & + & LE_{water} & + & LE_{town} & + & LE_{nature} \\
S^{\uparrow} & = & S^{\uparrow}_{sea} & + & S^{\uparrow}_{water} & + & S^{\uparrow}_{town} & + & S^{\uparrow}_{nature} \\
L^{\uparrow} & = & L^{\uparrow}_{sea} & + & L^{\uparrow}_{water} & + & L^{\uparrow}_{town} & + & L^{\uparrow}_{nature}
\end{array}
$$

For the natural surfaces, an 'aggregated' vegetation is used, viz a vegetation representative of all the species present in the grid mesh.
As an option, it will be possible to use the soil and vegetation scheme on the different landscape types present in the grid mesh. Then averaging the fluxes coming from each landscape type will give the flux coming from the natural part of the grid mesh. Only a limited number of landscape types will be available: forests, grassland, C3 type cropland, C4 type cropland, irrigated crops, bare soil, rocks and permanent snow. For each lanscape, there will be a temporal evolution of the surface variables independently of the other landscape types.

The fluxes coming from the urban area are themselves average of fluxes from the roofs, roads and walls (see TEB scheme hereafter).

The surface schemes used for the 4 main surface types are:

- over seas: a Charnock's formulation, with stationnary SST
- over inland waters: a Charnock's formulation, with stationnary temperature.
- over natural areas: an improved version of the Interactions Soil-Biosphere-Atmosphere (ISBA) scheme by Noilhan and Planton (1989), Noilhan and Mahfouf (1996), Calvet et al. (1998) and Boone et al. (1999),
- over artificial areas: the 'Town Energy Budget' scheme by Masson (2000).

6.2 Fluxes over water surfaces

6.2.1 Free water surfaces

For ocean surfaces and over inland waters, all the prognostic variables are kept constant.
The surface fluxes are calculated using Eqs. 6.89, 6.90, 6.92 and Eqs. 6.115, 6.116, 6.117, taking the relative humidity of the ocean $hu = 1$, and $veg = p_{sn} = 0$. The roughness length is given by Charnock's relation:

$$z_{0sea} = 0.015 \frac{u_*^2}{g} \tag{6.1}$$

6.2.2 Sea ice

Sea ice is detected in the model when sea surface temperature (SST) is two degrees below 0°C (i.e. 271.15K). In this case, in order to avoid an overestimation of the evaporation flux, the calculations are performed with the roughness length of flat snow surfaces:

$$z_{0ice} = 2.4 \ \times \ 10^{-4} m \tag{6.2}$$

In the same manner, the sea ice albedo is set equal to the fresh snow albedo instead of the free water albedo. This leads to a much brighter surface. This has no effect on the sea ice cover (since there is no evolution of the sea surface parameters), but modifies the lower boundary shortwave flux input for the atmospheric radiative scheme.

6.3 Urban and artificial areas: the TEB surface cheme

The Town Energy Budget (TEB) scheme is aimed to simulate the turbulent fluxes into the atmosphere at the surface of a mesoscale atmospheric model which is covered by buildings, roads, or any artificial material (see Masson 2000 for all details and equations). It should parameterize both the urban surface and the roughness sublayer, so that the atmospheric model only 'sees' a constant flux layer as its lower boundary. At mesoscale (with a grid mesh larger than a few hundred meters), spatial averaging of the town characteristics, as well as its effect on the atmosphere, are necessary. The individual shapes of each building are no longer taken into account. The TEB geometry is based on the canyon hypothesis. However, a single canyon would be too restrictive at the considered horizontal scale. We therefore use the following original city representation:

1. the buildings have the same height and width (in the model mesh). The roof level is at the surface level of the atmospheric model.

2. buildings are located along identical roads, the length of which is considered far greater than their width. The space contained between two facing buildings is defined as a canyon.

3. any road orientation is possible, and they all exist with the same probability. This hypothesis allows the computation of averaged forcing for road and wall surfaces. In other words, when the canyon orientation appears in a formula (with respect to the sun or the wind direction), it is averaged over 360°. In this way, no discretization is performed on the orientation.

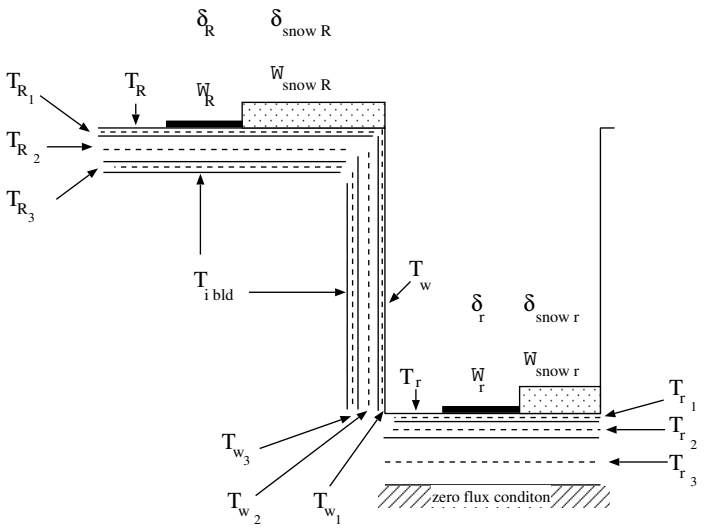

Figure 6.2: Canyon geometry in the TEB scheme ,and its prognostic variables.

These hypotheses, as well as the formulations chosen for the physics (see Masson 2000), allow the development of a relatively simple scheme. The parameters describing the city are displayed in Table 5.3 in chapter 5. The prognostic variables of the scheme are in Table 6.1. **The TEB model does not use one urban surface temperature** (representative of the entire urban cover), but **three** surface temperatures representative of roofs, roads and walls (see figure 6.2). There are two reasons for that:

- this allows to keep the maximum of results gathered by the urban climatologists about the urban surface energy budget,

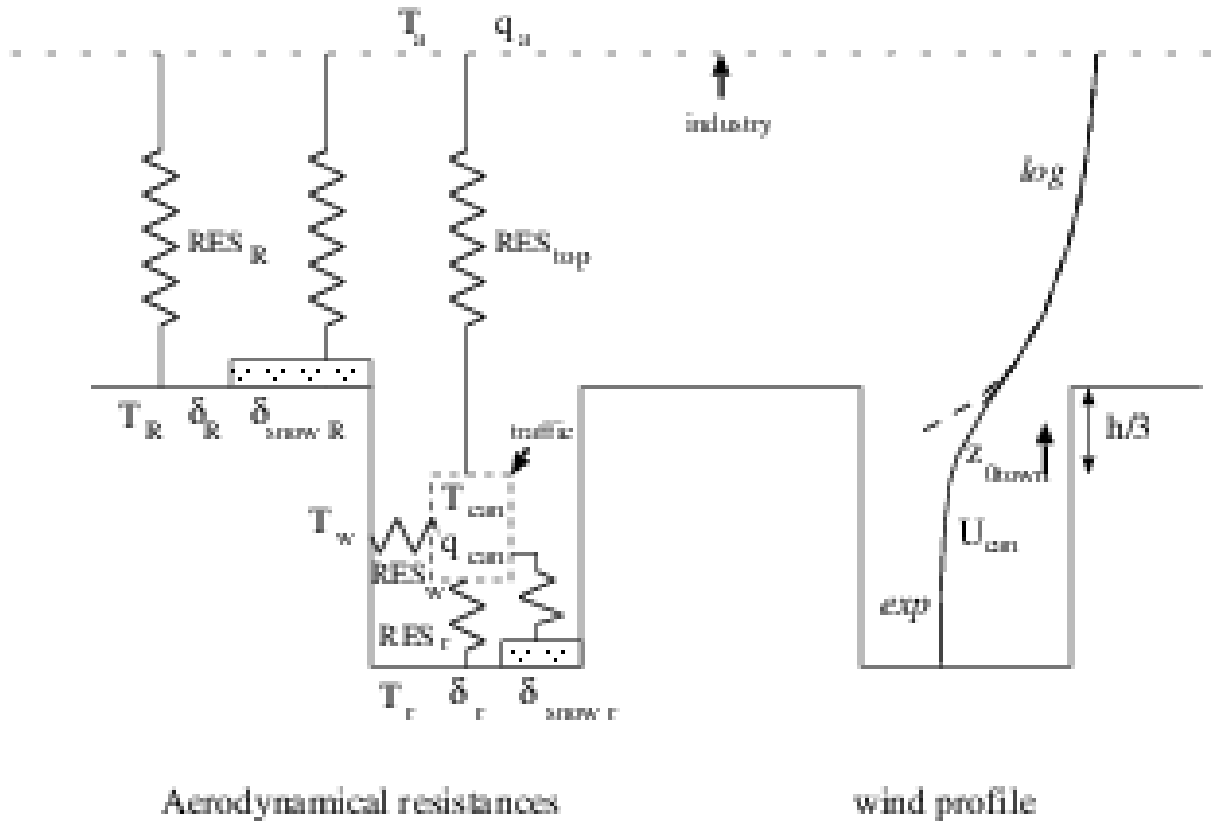

Figure 6.3: Energy fluxes between the artificial surfaces and the atmosphere.

- the use of only one temperature should be debatable, because it is observed that the Monin-Obukhov similarity theory does not apply for temperature in the urban roughness sublayer.

As a consequence, **three** surface energy budgets are computed, one for each surface type. The resulting fluxes at town scale are obtained by averaging (see figure 6.3 for the links between surfaces and atmosphere).

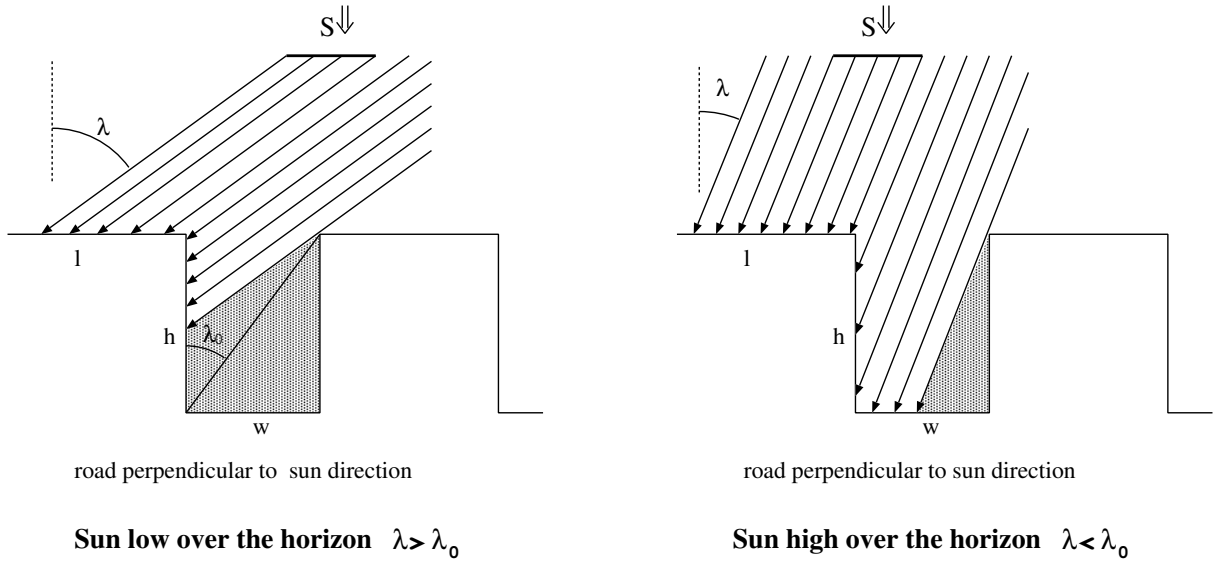

Figure 6.4: Solar radiation input for a road perpendicular to the sun azimuth. In the TEB scheme, the contribution of all the other road directions are averaged with this one.

The physics of the scheme are relatively complete, thanks to the use of this non-flat canyon geometry:

- interception of snow and water.
- longwave computations (with one reemission), infra-red trapping effect.
- shortwave computations (with an infinity of reflections), solar trapping effect. The solar zenith angle influences each surface energy input (see figure 6.4) and thus the trapping effect.
- momentum fluxes (with an urban roughness).
- sensible and latent heat fluxes, dew.
- storage flux (by explicit conduction equation), domestic heating (buildings internal temperature).
- anthropogenic fluxes (car traffic, factories).

symbol	designation of symbol	unit
prognostic variables		
T_{R_k}, T_{r_k}, T_{w_k}	temperature of the k^{th} roof, road or wall layer	K
W_R, W_r	roof and road water interception reservoir	kg m^{-2}
$W_{snow\,R}$, $W_{snow\,r}$	roof and road snow interception reservoir	kg m^{-2}
$T_{snow\,R}$, $T_{snow\,r}$	roof and road snow temperature	K
$\rho_{snow\,R}$, $\rho_{snow\,r}$	roof and road snow density	kg m^{-3}
$\alpha_{snow\,R}$, $\alpha_{snow\,r}$	roof and road snow albedo	-
diagnostic variables		
T_{can}	canyon air temperature	K
q_{can}	canyon air specific humidity	kg kg^{-1}
U_{can}	along canyon horizontal wind	m s^{-1}
α_{town}	town effective albedo	-
$T_{s_{town}}$	town area averaged radiative surface temperature	K
input energy fluxes		
$L^{\downarrow}$	downward infra-red radiation on an horizontal surface	W m^{-2}
$S^{\downarrow}$	downward **diffuse** solar radiation on an horizontal surface	W m^{-2}
$S^{\Downarrow}$	downward **direct** solar radiation on an horizontal surface	W m^{-2}
$H_{traffic}$	anthropogenic sensible heat flux released in the canyon	W m^{-2}
$LE_{traffic}$	anthropogenic latent heat flux released in the canyon	W m^{-2}
$H_{industry}$	anthropogenic sensible heat flux released by industries	W m^{-2}
$LE_{industry}$	anthropogenic latent heat flux released by industries	W m^{-2}
other energy input		
$T_{i_{bld}}$	building interior temperature	K
output energy fluxes		
S^*_R, S^*_r, S^*_w	net solar radiation budget for roofs, roads and walls	W m^{-2}
L^*_R, L^*_r, L^*_w	net infra-red radiation budget for roofs, roads and walls	W m^{-2}
H_R, H_r, H_w	turbulent sensible heat flux for roofs, roads and walls	W m^{-2}
LE_R, LE_r, LE_w	turbulent latent heat flux for roofs, roads and walls	W m^{-2}
$G_{R_{k,k+1}}$, $G_{r_{k,k+1}}$, $G_{w_{k,k+1}}$	conduction heat flux between k^{th} and $k+1^{th}$ roof, road or wall layers	W m^{-2}
H_{town}	town averaged turbulent sensible heat flux	W m^{-2}
LE_{town}	town averaged turbulent latent heat flux	W m^{-2}

Table 6.1: Energy fluxes and variables in the TEB scheme

The original TEB introduced by Masson (2000) is coupled to Meso-NH at the surface only (single-layer coupling; left panel of Fig. 6.5). This means that the mean building height is at the ground level of Meso-NH and the street level in the urban area is below the Meso-NH surface level. This modelling approach is suited for homogeneous low- and mid-rise cities, but becomes more problematic for heterogenous and high-rise cities. Therefore, a multi-layer coupling (right panel of Fig. 6.5) has been introduced by Schoetter et al. (2020). With the multi-layer coupling, the city ground level is the same as the ground level in Meso-NH, and the buildings are immersed in the atmospheric model. The prognostic variables of horizontal wind, subgrid turbulence kinetic energy, potential temperature, and water vapour mixing ratio are impacted by the buildings at all model levels which intersect the buildings.

The prognostic Meso-NH equations need to be modified for the multi-layer coupling. The friction exerted by the buildings on the horizontal wind components is taken into account using a drag force approach. The theoretical basis for this approach is explained in Raupach 1992. For highly three-dimensional flow over sparse roughness elements (e.g. the buildings in the urban roughness sublayer), the total turbulent stress can be written as the sum of the stress on the roughness elements and the stress on the underlying surface. This approach assumes that the wake and drag properties of an isolated roughness element can be characterised by an effective shelter area and volume. This

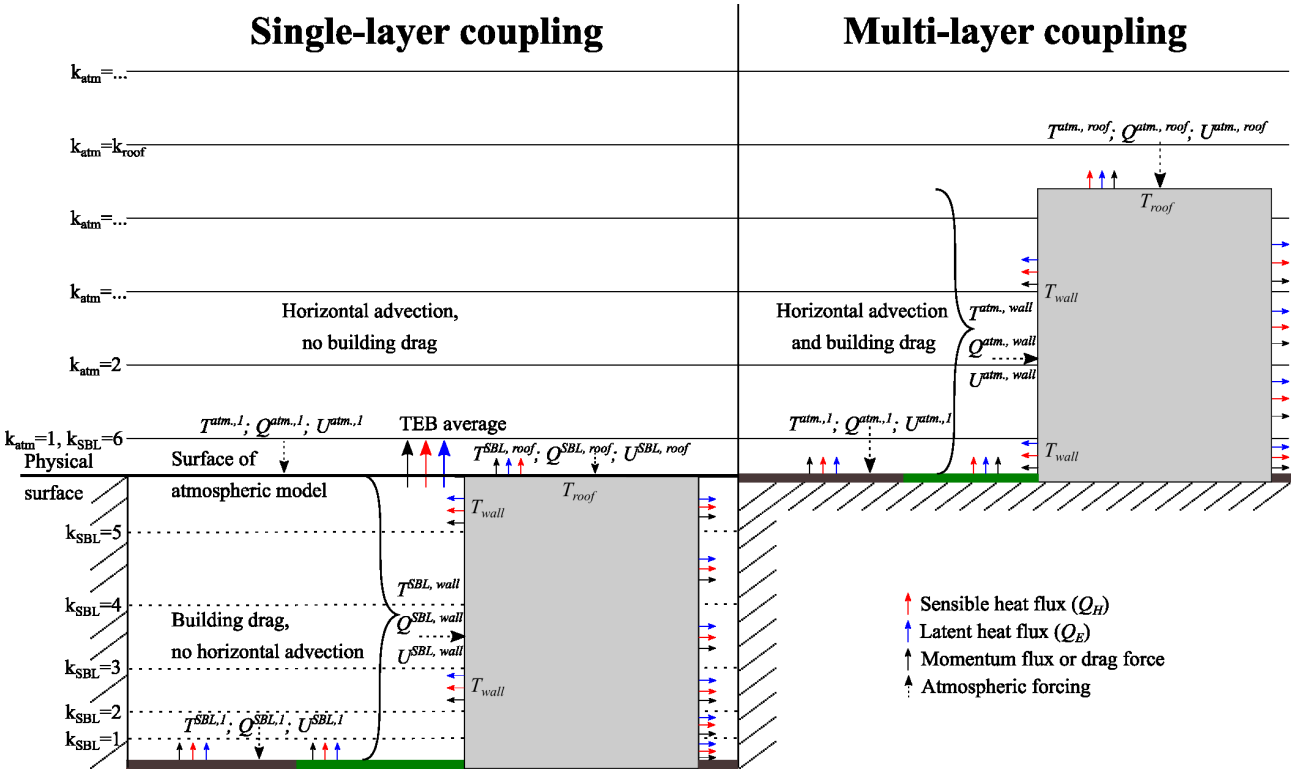

Figure 6.5: The single-layer and multi-layer approach for the coupling between Meso-NH and SURFEX-TEB. For the single-layer coupling, the urban canopy layer is located below the surface of the atmospheric model and the Surface Boundary Layer (SBL) scheme is used to calculate the profiles of the meteorological variables there. For the multi-layer coupling, the buildings are immersed in and interact directly with the atmosphere.

hypothesis is valid at low roughness density, but is unlikely to hold at high roughness density due to sheltering effects. For this reason, the drag force approach might yield uncertainties for high-density cities. The drag force approach translates into Equation 6.3 for the u component (similar for the v component).

$$\left.\frac{\partial(\rho_{deff}\, u)}{\partial t}\right|_{build} = -\rho_{deff}\, \left(c_d^{wall} d_{wall} + c_d^{roof} d_{roof}\right) u \mid \boldsymbol{u_{hor}} \mid \tag{6.3}$$

The horizontal wind speed ($\mid \boldsymbol{u_{hor}} \mid$) is calculated based on the prognostic u and v wind components (Equation 6.4).

$$\mid \boldsymbol{u_{hor}} \mid = \sqrt{u^2 + v^2} \tag{6.4}$$

The vertical frontal wall area density (d_{wall}) is calculated under the assumption that all buildings at grid point scale have the same height (Equation 6.5) to maintain coherence with the geometric assumption in TEB. A cylindrical building shape is assumed to calculate the frontal wall area density based on the wall to plan area ratio (λ_w). The real shape of the buildings is not taken into account, since this would require the definition of a large number of additional model input maps describing the frontal area density as a function of height and wind direction.

$$d_{wall}(z_k^m) = \begin{cases} \frac{\lambda_w}{\pi H_{bld}} & for \quad z_{k+1}^w < H_{bld} \\ \left(\frac{H_{bld} - z_k^w}{z_{k+1}^w - z_k^w}\right) \frac{\lambda_w}{\pi H_{bld}} & for \quad z_k^w < H_{bld} \leq z_{k+1}^w \\ 0 & else \end{cases} \tag{6.5}$$

The grid point average building height is denoted with H_{bld}. The height above ground of the k^{th} model level is z_k^m, the height above ground of the interfaces between the model levels is z_k^w.
The roofs are assumed to be horizontal. The vertical density of horizontal roofs (d_{roof}) is calculated following Equation 6.6.

$$d_{roof}(z_k^m) = \begin{cases} \frac{\lambda_p}{z_{k+1}^w - z_k^w} & for \;\; z_k^w < H_{bld} \leq z_{k+1}^w \\ 0 & else \end{cases} \tag{6.6}$$

The drag coefficient for the vertical walls (c_d^{wall}) is set to 0.4 since this corresponds to the value from wind tunnel studies reported by Raupach (1992) for cubes - a type of obstacles similar to actual buildings. The drag coefficient due to the roofs is calculated similar to Hamdi and Masson (2008) following Equations 6.7 and 6.8.

$$c_d^{roof} = \left(\frac{u_*^{roof}}{\mid \boldsymbol{u_{hor}}(\boldsymbol{z_{k,roof}^m}) \mid} \right)^2 \tag{6.7}$$

$$u_*^{roof} = \frac{\kappa \mid \boldsymbol{u_{hor}}(\boldsymbol{z_{k,roof}^m}) \mid}{ln\left(\frac{(z_{k,roof}^m - H_{bld})}{z_{0,m}^{roof}} \right)} \tag{6.8}$$

$z_{k,roof}^m$ is the height above ground of the level, at least 0.5 m above the roof. The von Kármán constant (κ) is 0.4, the momentum roughness length of the roof ($z_{0,m}^{roof}$) is assumed to be 0.15 m to represent chimneys, air conditioning systems, or other small constructions that are usually present on the roofs. Atmospheric stability is not taken into account in the calculation of the friction due to the roofs; it is assumed that the strong wind shear close to the roofs dominates the effects due to buoyancy.
The production of subgrid turbulent kinetic energy (e) due to the wind shear close to the buildings walls and roofs is considered in a similar manner as in Martilli et al. (2002), Chin et al. (2005), and Hamdi and Masson (2008), following Equation 6.9.

$$\left. \frac{\partial(\rho_{deff}\, e)}{\partial t} \right|_{build} = \rho_{deff} \left(c_d^{wall} d_{wall} + c_d^{roof} d_{roof} \right) \mid \boldsymbol{u_{hor}} \mid^3 \tag{6.9}$$

The tendencies of potential temperature and water vapour mixing ratio due to the sensible (Q_h^{wall}, Q_h^{roof}) and latent (Q_e^{wall}, Q_e^{roof}) heat fluxes from the walls and the roofs towards the atmosphere are calculated following Equations 6.10 and 6.11.

$$\left. \frac{\partial(\rho_{deff}(z_k^m)\, \theta(z_k^m))}{\partial t} \right|_{build} = \begin{cases} \frac{Q_h^{wall}}{C_p H_{bld}} & for \;\; z_{k+1}^w < H_{bld} \\ \left(\frac{H_{bld} - z_k^w}{z_{k+1}^w - z_k^w} \right) \frac{Q_h^{wall}}{C_p H_{bld}} + \frac{Q_h^{roof}}{C_{pd}(z_{k+1}^w - z_k^w)} & for \;\; z_k^w < H_{bld} \leq z_{k+1}^w \\ 0 & else \end{cases} \tag{6.10}$$

$$\left. \frac{\partial(\rho_{deff}(z_k^m)\, r_v(z_k^m))}{\partial t} \right|_{build} = \begin{cases} \frac{Q_e^{wall}}{L_i H_{bld}} & for \;\; z_{k+1}^w < H_{bld} \\ \left(\frac{H_{bld} - z_k^w}{z_{k+1}^w - z_k^w} \right) \frac{Q_e^{wall}}{L_i H_{bld}} + \frac{Q_e^{roof}}{L_i (z_{k+1}^w - z_k^w)} & for \;\; z_k^w < H_{bld} \leq z_{k+1}^w \\ 0 & else \end{cases} \tag{6.11}$$

Turbulent fluxes are in Wm^{-2} of total horizontal plan area of the grid point. They are calculated in the physical routines of TEB with respect to the potential temperature. The specific heat L_i is 2.5008e+6 Jkg^{-1} for evaporation and 2.8345e+6 Jkg^{-1} for sublimation.
The coupling between Meso-NH and SURFEX-TEB is technically modified such that SURFEX-TEB can receive the forcing from the first to the NC^{th} $(1 : NC)$ Meso-NH level. For the sake of simplicity, the horizontal dimensions of the Meso-NH variables are not explicitly given in the equations. The horizontal wind speed ($\mid \boldsymbol{u_{hor}} \mid$) is calculated based on the prognostic u and v wind components (Equation 6.12).

$$\mid \boldsymbol{u_{hor}}(\boldsymbol{z^m_{1:NC}}) \mid = \sqrt{u(z^m_{1:NC})^2 + v(z^m_{1:NC})^2} \tag{6.12}$$

The air temperature (T) is calculated based on the prognostic potential temperature (θ) and the Exner function (Φ) following

$$T(z^m_{1:NC}) = \theta(z^m_{1:NC})\Pi(z^m_{1:NC}) \tag{6.13}$$

$$\Pi(z^m_{1:NC}) = \left(\frac{p(z^m_{1:NC})}{p_{00}}\right)^{\frac{R_d}{C_p}} \tag{6.14}$$

where p is the diagnostic absolute pressure. The absolute humidity (q) is calculated based on the prognostic mixing ratio of water vapour (r_v) following

$$q(z^m_{1:NC}) = r_v(z^m_{1:NC})\ \rho_{deff}(z^m_{1:NC}) \tag{6.15}$$

and the density of the moist air (ρ) is given by

$$\rho(z^m_{1:NC}) = \frac{p(z^m_{1:NC})}{R_d T(z^m_{1:NC})} \frac{1 + (R_d/R_v) r_v(z^m_{1:NC})}{1 + r_v(z^m_{1:NC})} \tag{6.16}$$

The height of the atmospheric forcing level used by SURFEX-TEB ($z_{k,forc.}$) needs to be calculated based on the height of the Meso-NH levels (z^m_k). It is ambiguous whether this forcing height should be the distance of the atmospheric level to the potentially inclined surface (inclination angle α) or the vertical height above the surface. It is assumed that for katabatic winds located in the first few meters above ground level (a.g.l.), the distance to the surface is the most relevant, whereas for the other processes it will be the vertical height above the surface. Therefore, the forcing height is defined as the shortest distance between the model level and the surface in the lowest 5 m vertical distance to the surface, and as the vertical distance at or above 20 m vertical distance to the surface (Equation 6.17). A linear transition is applied in between (Equations 6.17 and 6.18).

$$z_{k,forc.} = f_k z^m_k + (1 - f_k) z^m_k cos(\alpha) \tag{6.17}$$

$$f_k = min\left(1.0, \frac{max(z^m_k - 5.0, 0.0)}{15.0}\right) \tag{6.18}$$

The multi-layer coupling of TEB is technically enabled by a logical switch which deactivates the prognostic equations of the SBL scheme of Hamdi and Masson (2008) and instead at each time step fills the SBL scheme's prognostic variables with the corresponding Meso-NH variables. With this implementation it is easy to switch between the single-layer and the multi-layer coupling. The

meteorological forcing for the impervious surfaces such as roads ($imp.$), which have an aerodynamic roughness length of 0.05 m, and the low urban vegetation ($lveg.$) is taken from the first Meso-NH level following

$$U_{forc.}^{imp./lveg.} = \mid \boldsymbol{u_{hor}}(1) \mid ; \;\; T_{forc.}^{imp./lveg.} = T(1) \; ; \;\; Q_{forc.}^{imp./lveg.} = \frac{q(1)}{\rho(1)} \tag{6.19}$$

where Q denotes the specific humidity, U the wind speed, and the height of the forcing is given by

$$z_{forc.}^{imp./lveg.} = z_{1,forc.} \tag{6.20}$$

The meteorological forcing for the roof (Equation 6.21) is taken from the closest Meso-NH level, but at least 0.5 m above the roof (k_{roof}).

$$U_{forc.}^{roof} = \mid \boldsymbol{u_{hor}}(k_{roof}) \mid ; \;\; T_{forc.}^{roof} = T(k_{roof}) \; ; \;\; Q_{forc.}^{roof} = \frac{q(k_{roof})}{\rho(k_{roof})} \tag{6.21}$$

The height of the forcing above the roof is

$$z_{forc.}^{roof} = z_{k_{roof},forc.} - H_{bld} \tag{6.22}$$

Since in TEB the walls are not vertically discretised, there is only one value for the prognostic wall temperature at grid point scale, hence the average value of the meteorological forcing variables is calculated for all Meso-NH levels intersecting the walls (Equations 6.23 to 6.25).

$$U_{for}^{wall} = \frac{1}{H_{bld}} \sum_{k=1}^{k_{roof}} \begin{cases} \mid \boldsymbol{u_{hor}}(k) \mid (z_{k+1}^{w} - z_{k}^{w}) & for \quad z_{k+1}^{w} \leq H_{bld} \\ \mid \boldsymbol{u_{hor}}(k) \mid (H_{bld} - z_{k}^{w}) & for \quad z_{k}^{w} < H_{bld} < z_{k+1}^{w} \end{cases} \tag{6.23}$$

$$T_{for}^{wall} = \frac{1}{H_{bld}} \sum_{k=1}^{k_{roof}} \begin{cases} T(k)(z_{k+1}^{w} - z_{k}^{w}) & for \quad z_{k+1}^{w} \leq H_{bld} \\ T(k)(H_{bld} - z_{k}^{w}) & for \quad z_{k}^{w} < H_{bld} < z_{k+1}^{w} \end{cases} \tag{6.24}$$

$$Q_{for}^{wall} = \frac{1}{H_{bld}} \sum_{k=1}^{k_{roof}} \begin{cases} \frac{q(k)}{\rho(k)}(z_{k+1}^{w} - z_{k}^{w}) & for \quad z_{k+1}^{w} \leq H_{bld} \\ \frac{q(k)}{\rho(k)}(H_{bld} - z_{k}^{w}) & for \quad z_{k}^{w} < H_{bld} < z_{k+1}^{w} \end{cases} \tag{6.25}$$

The sensible and latent heat fluxes from the roof, walls, impervious and pervious surfaces to the air in the street canyon are then calculated with the same formulas that are detailed in Hamdi and Masson (2008) and Lemonsu et al. (2012).

6.4 Soil and Vegetation

6.4.1 Treatment of the soil heat content

The prognostic equations for the surface temperature T_s and its mean value T_2 over one day τ, are obtained from the force-restore method proposed by Bhumralkar (1975) and Blackadar (1976):

$$\frac{\partial T_s}{\partial t} = C_T(R_n - H - LE) - \frac{2\pi}{\tau}(T_s - T_2), \tag{6.26}$$

$$\frac{\partial T_2}{\partial t} = \frac{1}{\tau}(T_s - T_2), \tag{6.27}$$

where H and LE are the sensible and latent heat fluxes, and R_n is the net radiation at the surface. The surface temperature T_s evolves due to both the diurnal forcing by the heat flux $G = R_n - H - LE$ and a restoring term towards its mean value T_2. In contrast, the mean temperature T_2 only varies according to a slower relaxation towards T_s.
The coefficient C_T is expressed by

$$C_T = 1/\left(\frac{(1-veg)(1-p_{sng})}{C_g} + \frac{veg(1-p_{snv})}{C_v} + \frac{p_{sn}}{C_s}\right) \tag{6.28}$$

where veg is the fraction of vegetation, C_g is the ground heat capacity, C_s is the snow heat capacity, C_v is the vegetation heat capacity, and

$$p_{sng} = \frac{W_s}{W_s + W_{crn}}; \qquad p_{snv} = \frac{h_s}{h_s + 5000 z_0}; \qquad p_{sn} = (1-veg)p_{sng} + vegp_{snv} \tag{6.29}$$

are respectively the fractions of the bare soil and vegetation covered by snow, and the fraction of the grid covered by snow. Here, $W_{crn} = 10\ mm$, and $h_s = W_s/\rho_s$ is the thickness of the snow canopy (ρ_s is the snow density). The partitioning of the grid into bare soil, vegetation, and snow regions, is indicated in Fig.(6.6) .

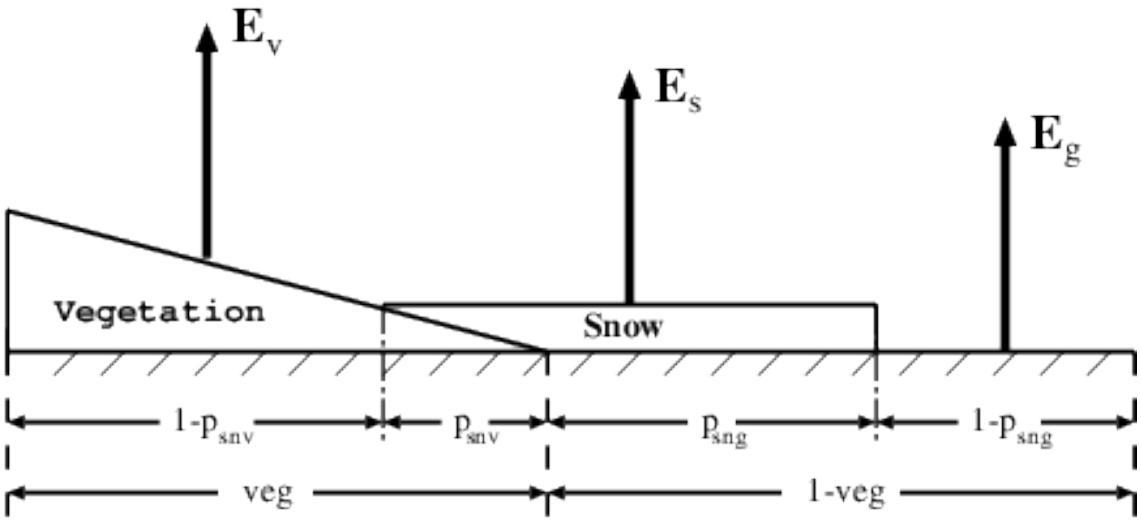

Figure 6.6: Partitioning of the grid

The heat capacities of the ground and snow canopies are respectively given by

$$C_g = C_{gsat}\left(\frac{w_{sat}}{w_2}\right)^{b/2log10} ; C_g \leq 1.5 \times 10^{-5}\ Km^2J^{-1} \tag{6.30}$$

where G_{gsat} is the heat capacity at saturation, and w_{sat} the volumetric moisture content of the soil at saturation; and

$$C_s = 2 \times \left(\frac{\pi}{\lambda_s c_s \tau}\right)^{1/2} \tag{6.31}$$

where $\lambda_s = \lambda_i \times {\rho_s}^{1.88}$; $c_s = c_i(\rho_s/\rho_i)$: λ_i is the ice conductivity; c_i is the heat capacity of ice; and ρ_i is the relative density of ice (see Douville 1994, Douville et al. 1995).

After an intermediate surface temperature ${T_s}^*$ is evaluated from Eq. (6.26), the cooling due to the melting of snow is considered following

$${T_s}^+ = {T_s}^* - C_T L_f(melt)\Delta t \tag{6.32}$$

where L_f is the latent of fusion, Δt is the timestep, and the melting rate of snow is

$$melt = p_{sn}\left(\frac{T_n - T_0}{C_s L_f \Delta t}\right); \quad melt \geq 0 \tag{6.33}$$

Here,
$T_0 = 273.16\ K$;
$T_n = (1 - veg){T_s}^* + veg T_2$
Similarly, the intermediate mean temperature ${T_2}^*$ obtained from Eq. (2) is also modified due to the melting/freezing of water in the soil layer occurring for temperatures between $-5°C$ and $0°C$. The resulting mean temperature is

$${T_2}^+ = {T_2}^* + (\Delta w_2)_{frozen} L_f C_g d \tag{6.34}$$

with

$$(\Delta w_2)_{frozen} = \left[1 - \left(\frac{{T_2}^* - 268.16}{5.}\right)\right](w_2(t) - w_2(t - \Delta t)) \tag{6.35}$$

$$(\Delta w_2)_{frozen} = 0 \quad if\ T_2 \leq -5°C\ or\ if\ T_2 \geq 0°C \tag{6.36}$$

where $d = 15\ cm$ is an estimated average of the penetration of the diurnal wave into the soil. Only the mean temperature T_2 is modified by this factor. The surface temperature T_s, however, indirectly feels this effect through the relaxation term in Eq. (1).

6.4.2 Treatment of the soil water

Equations for w_g and w_2 are derived from the force-restore method applied by Deardorff (1977) to the ground soil moisture:

$$\frac{\partial w_g}{\partial t} = \frac{C_1}{\rho_w d_1}(P_g - E_g) - \frac{C_2}{\tau}(w_g - w_{geq})\ ; 0 \leq w_g \leq w_{sat} \tag{6.37}$$

$$\frac{\partial w_2}{\partial t} = \frac{1}{\rho_w d_2}(P_g - E_g - E_{tr}) - \frac{C_3}{d_2 \tau}\ max\left[0., (w_2 - w_{fc})\right]; 0 \leq w_2 \leq w_{sat} \tag{6.38}$$

where P_g is the flux of liquid water reaching the soil surface (including the melting), E_g is the evaporation at the soil surface, E_{tr} is the transpiration rate, ρ_w is the density of liquid water, and d_1 is an arbitrary normalization depth of 10 centimeters. In the present formulation, all the liquid water from the flux P_g goes into the reservoirs w_g and w_2, even when snow covers fractions of the ground and vegetation. The first term on the right hand side of Eq. (12) represents the influence of surface atmospheric fluxes when the contribution of the water extraction by the roots is neglected. The coefficients C_1 and C_2, and the equilibrium surface volumetric moisture w_{geq}, have been calibrated for different soil textures and moistures.
The expression for C_1 differs depending on the moisture content of the soil. For wet soils (i.e., $w_g \geq w_{wilt}$), this coefficient is expressed as

$$C_1 = C_{1sat} \left(\frac{w_{sat}}{w_g} \right)^{b/2+1} \tag{6.39}$$

For dry soils (i.e., $w_g < w_{wilt}$), the vapor phase transfer needs to be considered in order to reproduce the physics of water exchange. These transfers are parameterized as a function of the wilting point w_{wilt}, the soil water content w_g, and the surface temperature T_s, using the Gaussian expression (see Braud et al. 1993, Giordani 1993)

$$C_1 = C_{1max} exp \left[-\frac{(w_g - w_{max})^2}{2\sigma^2} \right] \tag{6.40}$$

where w_{max}, C_{1max}, and σ are respectively the abscissa of the maximum, the mode, and the standard deviation of the Gaussian functions (see Appendix B). The other coefficient, C_2, and the equilibrium water content, w_{geq}, are given by

$$C_2 = C_{2ref} \left(\frac{w_2}{w_{sat} - w_2 + 0.01} \right) \tag{6.41}$$

$$w_{geq} = w_2 - a w_{sat} \left(\frac{w_2}{w_{sat}} \right)^p \left[1 - \left(\frac{w_2}{w_{sat}} \right)^{8p} \right] \tag{6.42}$$

For the w_g evolution, Eq. (13) represents the water budget over the soil layer of depth d_2. The drainage, which is proportional to the water amount exceeding the field capacity (i.e., $w_2 - w_{fc}$), is considered in the second term of the equation (see Mahfouf et al. 1994). The coefficient C_3 does not depend on w_2 but simply on the soil texture (see Appendix A). Similarly, run-off occurs when w_g or w_2 exceeds the saturation value w_{sat}.

Root zone soil layer option

In the standard two-soil layer version of ISBA, it is not possible to distinguish the root zone and sub-root zone soil water reservoirs. With the three-layer version, the deep soil layer may provide water to the system through capillary rises only, and the available water content (for transpiration) is clearly defined.
The bulk soil layer (referred to as w_2 in the previous sections) is divided into a root-zone layer (with a depth d_2) and base-flow layer (with a thickness defined as $d_3 - d_2$). The governing equations for the time evolution of soil moisture for the two sub-surface soil layers are written following (Boone

et al. 1999) as

$$\frac{\partial w_2}{\partial t} = \frac{1}{\rho_w d_2}\left(P_g - E_g - E_{tr}\right) - \frac{C_3}{d_2\tau}\max\left[0,\ (w_2 - w_{fc})\right] - \frac{C_4}{\tau}\left(w_2 - w_3\right) \quad (6.43)$$

$$\frac{\partial w_3}{\partial t} = \frac{d_2}{(d_3 - d_2)}\left\{\frac{C_3}{d_2\tau}\max\left[0,\ (w_2 - w_{fc})\right] + \frac{C_4}{\tau}\left(w_2 - w_3\right)\right\} \quad (6.44)$$

$$- \frac{C_3}{(d_3 - d_2)\,\tau}\max\left[0,\ (w_3 - w_{fc})\right]\ ; \qquad 0 \le w_3 \le w_{sat} \quad (6.45)$$

where C_4 represents the vertical diffusion coefficient. It is defined as

$$C_4 = C_{4\,ref}\,\overline{w}_{2,3}{}^{C_{4b}} \quad (6.46)$$

$$(6.47)$$

where $\overline{w}_{2,3}$ represents the interpolated volumetric water content representative of the values at the layer interface (d_2). The $C_{4\,ref}$ and C_{4b} coefficients are defined using the soil sand and clay contents, consistent with the other model parameters (see the section on model coefficients). In addition, the $C_{4\,ref}$ coefficient is scaled as a function of grid geometry. The equations are integrated in time using a fully implicit method.

6.4.3 Treatment of the intercepted water

Rainfall and dew intercepted by the foliage feed a reservoir of water content W_r. This amount of water evaporates in the air at a potential rate from the fraction δ of the foliage covered with a film of water, as the remaining part $(1-\delta)$ of the leaves transpires. Following Deardorff (1978), we set

$$\frac{\partial W_r}{\partial t} = vegP - (E_v - E_{tr}) - R_r\ ;\ 0 \le W_r \le W_{rmax} \quad (6.48)$$

where P is the precipitation rate at the top of the vegetation, E_v is the evaporation from the vegetation including the transpiration E_{tr} and the direct evaporation E_r when positive, and the dew flux when negative (in this case $E_{tr} = 0$), and R_r is the runoff of the interception reservoir. This runoff occurs when W_r exceeds a maximum value W_{rmax} depending upon the density of the canopy, i.e., roughly proportional to $vegLAI$. According to Dickinson (1984), we use the simple equation:

$$W_{rmax} = 0.2 vegLAI \quad [mm] \quad (6.49)$$

6.4.4 Treatment of soil ice

The inclusion of soil freezing necessitates the addition of so-called phase change to the thermal and hydrologic transfer equations. In addition, a freezing/drying wetting/thawing analogy is used to model changes in the force-restore coefficients so that they must also be modified accordingly. Terms which have been added to the baseline ISBA scheme are underlined in this section, while terms which are modified are denoted using an $*$ superscript. Additional details related to soil freezing scheme can be found in Boone et al. (2000).

The basic prognostic equations including soil ice are expressed as

$$\frac{\partial T_s}{\partial t} = C_T{}^* \left[R_n - H - LE^* - L_f(M_s - \underline{F_{g\,w}}) \right] - \frac{2\pi}{\tau}(T_s - T_2) \ , \tag{6.50}$$

$$\frac{\partial T_2}{\partial t} = \frac{1}{\tau}(T_s - T_2) + C_G{}^* L_f \underline{F_{2\,w}} \ , \tag{6.51}$$

$$\frac{\partial w_g}{\partial t} = \frac{1}{d_1 \rho_w} \left[C_1{}^* \left(P_g - E_{g\,l} + M_s \right) - \underline{F_{g\,w}} \right] - \frac{C_2{}^*}{\tau}(w_g - w_{g\,\mathrm{eq}}{}^*) \tag{6.52}$$

$$(w_{\min} \leq w_g \leq w_{\mathrm{sat}} - w_{g\,f}) \ , \tag{6.53}$$

$$\frac{\partial w_2}{\partial t} = \frac{1}{d_p \rho_w} \left(P_g - E_{g\,l} - E_{tr}{}^* + M_s - \underline{F_{2\,w}} \right) - \frac{C_3}{\tau} \max(0\,,\ w_2 - w_{\mathrm{fc}}{}^*) \tag{6.54}$$

$$(w_{\min} \leq w_2 \leq w_{\mathrm{sat}} - w_{2\,f}) \ , \tag{6.55}$$

$$\frac{\partial w_{g\,f}}{\partial t} = \frac{1}{d_1 \rho_w} \left(F_{g\,w} - E_{g\,f} \right) \qquad (0 \leq w_{g\,f} \leq w_{\mathrm{sat}} - w_{\min}) \ , \tag{6.56}$$

$$\frac{\partial w_{2\,f}}{\partial t} = \frac{1}{(d_2 - d_1)\,\rho_w} F_{2\,w} \qquad (0 \leq w_{2\,f} \leq w_{\mathrm{sat}} - w_{\min}) \ . \tag{6.57}$$

where $w_{g\,f}$ and $w_{2\,f}$ represent the volumetric soil ice content ($\mathrm{m}^3\ \mathrm{m}^{-3}$) in the surface and deep-soil reservoirs, respectively. The phase change mass and heat sink (source) terms (F; $\mathrm{kg\ m^{-2}\ s^{-1}}$) are expressed as

$$F_{g\,w} = (1 - p_{sng})\ (F_{g\,f} - F_{g\,m}) \ , \tag{6.58}$$

$$F_{2\,w} = (1 - p_{sng})\ (F_{2\,f} - F_{2\,m}) \ , \tag{6.59}$$

where the m and f subscripts represent melting and freezing, respectively. The freezing and melting phase change terms are formulated using simple relationships based on the potential energy available for phase change. They are expressed for the surface soil layer as

$$F_{g\,f} = (1/\tau_i)\ \min\left[K_s\, \epsilon_{s\,f} \max(0,\ T_0 - T_s)/C_I\, L_f,\ \rho_w\, d_1\ (w_g - w_{\min}) \right] \ , \tag{6.60}$$

$$F_{g\,m} = (1/\tau_i)\ \min\left[K_s\, \epsilon_{s\,m} \max(0,\ T_s - T_0)/C_I\, L_f,\ \rho_w\, d_1\, w_{g\,f} \right] \ , \tag{6.61}$$

and for the deep soil layer as

$$F_{2\,f} = (\delta_{2\,f}/\tau_i)\ \min\left[\epsilon_{2\,f} \max(0,\ T_0 - T_2)/C_I\, L_f,\ \rho_w\ (d_2 - d_1)\,(w_2 - w_{\min}) \right] \ , \tag{6.62}$$

$$F_{2\,m} = (1/\tau_i)\ \min\left[\epsilon_{2\,m} \max(0,\ T_2 - T_0)/C_I\, L_f,\ \rho_w\ (d_2 - d_1)\ w_{2\,f} \right] \ . \tag{6.63}$$

The characteristic time scale for freezing is represented by τ_i (s). The phase change efficiency coefficients, ϵ, introduce a dependence on the water mass available for phase changes which are expressed as the ratio of the liquid volumetric water content to the total soil porosity for freezing, and the ratio of ice content to the porosity for melting. The ice thermal inertia coefficient is defined as $C_I = 2(\pi/\lambda_i\, C_i \rho_i \tau)^{1/2}$ ($\mathrm{J\ m^{-2}\ K^{-1}}$). The insulating effect of vegetation is modeled using a coefficient defined as

$$K_s = \left(1 - \frac{veg}{K_2} \right) \left(1 - \frac{LAI}{K_3} \right) \ , \tag{6.64}$$

where the dimensionless coefficients have the values $K_2 = 5.0$ and $K_3 = 30.0$ (Giard and Bazile 1999). The most direct effect of vegetation cover is to slow the rate of phase changes for

more dense vegetation cover as energy not used for phase change is assumed to cool/warm the vegetative portion of the lumped soil-vegetation layer.
The deep-soil phase change (freezing) term is multiplied by a factor ($\delta_{2\,f}$) which essentially limits ice production during prolonged cold periods. It is defined as 0 if $z_f \geq z_{f\,\max}$ where

$$z_{f\,\max} = 4/\left(C_G{}^* c_g\right) \tag{6.65}$$

and the actual depth of ice in the soil is defined as

$$z_f = d_2 \left(\frac{w_{2\,f}}{w_{2\,f} + w_2}\right) \qquad (0 \leq z_f < d_2) \tag{6.66}$$

Ice is assumed to become part of the solid soil matrix. This is accomplished by defining the modified porosity (eg. Johnsson and Lundin 1991) as

$$w_{sat}{}^* = w_{sat} - w_{j\,f} \tag{6.67}$$

where j corresponds to the surface (g) or sub-surface (2) soil water reservoirs. This, in turn, is used to modify the force-restore coefficients (see Boone at al. 2000 for more details).

6.4.5 Treatment of the snow

One-layer snow scheme option

The evolution of the equivalent water content of the snow reservoir is given by

$$\frac{\partial W_s}{\partial t} = P_s - E_s - melt \tag{6.68}$$

where P_s is the precipitation of snow, and E_s is the sublimation from the snow surface.
The presence of snow covering the ground and vegetation can greatly influence the energy and mass transfers between the land surface and the atmosphere. Notably, a snow layer modifies the radiative balance at the surface by increasing the albedo. To consider this effect, the albedo of snow α_s is treated as a new prognostic variable. Depending if the snow is melting or not, α_s decreases exponentially or linearly with time.
If there is no melting (i.e., $melt = 0$):

$$\alpha_s(t) = \alpha_s(t - \Delta t) - \tau_a \frac{\Delta t}{\tau} + \frac{P_s \Delta t}{W_{crn}}(\alpha_{smax} - \alpha_{smin}) \tag{6.69}$$

$$\alpha_{smin} \leq \alpha_s \leq \alpha_{smax} \tag{6.70}$$

where $\tau_a = 0.008$ is the linear rate of decrease per day, $\alpha_{smin} = 0.50$ and $\alpha_{smax} = 0.85$ are the minimum and maximum values of the snow albedo.
If there is melting (i.e., $melt > 0$):

$$\alpha_s(t) = \left[\alpha_s(t - \Delta t) - \alpha_{smin}\right] exp\left[-\tau_f \frac{\Delta t}{\tau}\right] + \alpha_{smin} + \frac{P_s \Delta t}{W_{crn}}(\alpha_{smax} - \alpha_{smin}) \tag{6.71}$$

$$\alpha_{smin} \leq \alpha_s \leq \alpha_{smax} \tag{6.72}$$

where $\tau_f = 0.24$ is the exponential decrease rate per day. Of course, the snow albedo increases as snowfalls occur, as shown by the second terms of Eqs. (21) and (23).

The average albedo of a model grid-area is expressed as

$$\alpha_t = (1 - p_{sn})\alpha + p_{sn}\alpha_s \tag{6.73}$$

Similarly, the average emissivity ϵ_t is also influenced by the snow coverage:

$$\epsilon_t = (1 - p_{sn})\epsilon + p_{sn}\epsilon_s \tag{6.74}$$

where $\epsilon_s = 1.0$ is the emissivity of the snow. Thus, the overall albedo and emissivity of the ground for infrared radiation is enhanced by snow.
Because of the significant variability of thermal properties related with the snow compactness, the relative density of snow ρ_s is also considered as a prognostic variable. Based on Verseghy (1991), ρ_s decreases exponentially at a rate of τ_f per day:

$$\rho_s(t) = [\rho_s(t - \Delta t) - \rho_{smax}]\, exp\left[-\tau_f \frac{\Delta t}{\tau}\right] + \rho_{smax} + \frac{P_s \Delta t}{W_s}\rho_{smin} \tag{6.75}$$

$$\rho_{smin} \leq \rho_s \leq \rho_{smax} \tag{6.76}$$

where $\rho_{smin} = 0.1$ and $\rho_{smax} = 0.3$ are the minimum and maximum relative density of snow.
Finally, the average roughness length z_{0t} is

$$z_{0t} = (1 - p_{snz0})z_0 + p_{snz0}z_{0s} \tag{6.77}$$

where

$$p_{snz0} = \frac{W_s}{W_s + W_{crn} + \beta_s g z_0} \tag{6.78}$$

Here, $\beta_s = 0.408\ s^2 m^{-1}$ and $g = 9.80665\ ms^{-2}$ are physical constants, whereas z_{0s} is the roughness length of the snow.

Multi-layer snow scheme option

An additional snow scheme option has been added to ISBA. It is a so-called intermediate complexity scheme which is representative of a class of snow models which use several layers and have simplified physical parameterization schemes based on those of the highly detailed internal-process models while having computational requirements more closely resembling the relatively simple composite/force-restore or single layer schemes (eg.s Loth et al. 1993; Lynch-Steiglitz 1994; Sun et al. 1999). Compared to the baseline ISBA snow scheme, the explicit multi-layered approach resolves the large thermal and the density gradients which can exist in the snow cover, distinguishes the surface energy budgets of the snow and non-snow covered portions of the surface, includes the effects of liquid water storage in the snow cover, models the absorption of incident radiation within the pack, and calculates explicit heat conduction between the snow and the soil.
The conservation equation for the total snow cover mass is expressed as

$$\frac{\partial W_s}{\partial t} = P_s + p_{sn}\ (P - P_s) - E_s - E_{sl} - Q_n\ \ , \tag{6.79}$$

where E_{sl} represents evaporation of liquid water from the snow surface, and the product $p_{sn}\ (P - P_s)$ represents the portion of the total rainfall that is intercepted by the snow surface while the remaining rainfall is assumed to be intercepted by the snow-free soil and vegetation

canopy. The snow-runoff rate, Q_n, is the rate at which liquid water leaves the base of the snow cover.
The snow state variables are the heat content (H_s), the layer thickness (D), and the layer average density (ρ_s). The temperature (T_{sn}) and liquid water content (w_{sl}) are defined using the heat content. The total snow depth, D_s (m) is defined as

$$D_s = \sum_{i=1}^{N_s} D_i \tag{6.80}$$

where a three-layer configuration is currently used by default (i.e. $N_s = 3$). The surface snow layer is always less than or equal to 0.05 m, and this temperature is used to calculate the fluxes between the atmosphere and the snow surface. The snow density is compacted using standard empirical relationships (Anderson 1976). Additional changes arise to snowfall which generally reduces the snow density, and densification resulting from ripening. The snow heat content (J m^{-2}) is defined as

$$H_{s\,i} = c_{s\,i}\, D_i\ (T_{sn\,i} - T_0)\ -\ L_f\, \rho_w\, (w_{s\,i} - w_{sl\,i})\ \ , \tag{6.81}$$

where w_s is the total snow layer water equivalent depth (m), w_{sl} is the snow layer liquid water content (m), and c_s is the snow heat capacity (J m^{-3} K^{-1}) (using the same definition as the baseline ISBA snow scheme). The snow heat content is used in order to allow the presence of either cold (dry) snow which has a temperature less than or equal to the freezing point or warm (wet) snow which is characterized by a temperature at the freezing point and contains water in liquid form. The snow temperature and liquid water content can then be defined as

$$T_{sn\,i} \ = \ T_f\ +\ (H_{s\,i} + L_f\, \rho_w\, w_{s\,i})\,/\,(c_{s\,i}\, D_i)\ ; \qquad w_{l\,i} = 0 \tag{6.82}$$

$$w_{sl\,i} \ = \ w_{s\,i}\ +\ (H_{s\,i}/L_f\, \rho_w)\ ; \qquad T_{sn\,i} = T_f \ \text{ and } \ w_{sl\,i} \leq w_{sl\,\max i} \tag{6.83}$$

where $w_{sl\,\max i}$ is the maximum liquid water holding capacity of a snow layer, which is based on empirical relations. All water exceeding this flows into the layer below where it can do one or all of the following; add to the liquid water content, refreeze, or continue flowing downward.
Snow heat flow is along the thermal gradient as any snow melt or percolated water within the snow cover is assumed to have zero heat content. The layer-averaged snow temperature equation ($T_{s\,i}$) is expressed as

$$c_{s\,i} D_i \frac{\partial T_{sn\,i}}{\partial t} = G_{s\,i-1} - G_{s\,i} + R_{s\,i-1} - R_{s\,i} - S_{s\,i}\ \ , \tag{6.84}$$

where S_s represents an energy sink/source term associated with phase changes between the liquid and solid phases of water. Incoming short wave radiation (R_s) transmission within the snowpack decreases exponentially with increasing snow depth. At the surface, it is expressed as

$$R_{s\,0} = R_g\ (1 - \alpha_s) \tag{6.85}$$

where the snow albedo is defined using the same relationships as in the baseline version of ISBA (Douville et al. 1995). The sub-surface heat (G_s) flux terms are evaluated using simple diffusion. At the surface, this flux is expressed as

$$G_{s\,0} = \epsilon_s \left(R_A - \sigma_{SB} {T_{sn\,1}}^4\right)\ -\ H\,(T_{sn\,1})\ -\ LE\,(T_{sn\,1})\ -\ c_w\, p_{sn}\,(P - P_s)\,(T_f - T_r)\ \ , \tag{6.86}$$

The last term on the right hand side of the above equation represents a latent heat source when rain with a temperature (T_r) greater than T_0 falls on the snow cover, where c_w represents the heat capacity of water (4187 J kg^{-1} K^{-1}). Rainfall is simply assumed to have a temperature which is the larger of the air temperature (T_a) and the freezing point. The latent heat flux from the snow includes the liquid fraction weighted contributions from the evaporation of liquid water and sublimation. The ISBA surface soil/vegetation layer temperature is then coupled to the snow scheme using

$$\frac{1}{C_T}\frac{\partial T_s}{\partial t} = (1-p_n)\left[R_g\,(1-\alpha) + \epsilon_t\left(R_A - \sigma {T_s}^4\right) - H - LE - \frac{2\pi}{C_T \tau}\,(T_s - T_2)\right] \quad (6.87)$$

$$+ p_n\,\left[G_{s\,N} + R_{s\,N} + c_w\,Q_n\,\left(T_f - T_s\right)\right] \quad . \quad (6.88)$$

The term on the right hand side of the above equation involving the snow runoff (Q_n) represents an advective term. The net surface fluxes to/from the atmosphere are then calculated as the snow-cover fraction weighted sums over the snow and non-snow covered surfaces. When the 3-layer option is in use, the default ISBA scheme is used when the snow cover is relatively thin (arbitrarily defined as 0.05 m depth). When the snow depth exceeds this threshold, the snow mass and heat is transferred to the multi-layer scheme. This prevents numerical difficulties for vanishingly thin snow packs.

6.4.6 The surface fluxes

Only one energy balance is considered for the whole system ground-vegetation-snow (when the 3-layer snow scheme option is not in use). As a result, heat and mass transfers between the surface and the atmosphere are related to the mean values T_s and w_g.
The net radiation at the surface is the sum of the absorbed fractions of the incoming solar radiation R_G and of the atmospheric infrared radiation R_A, reduced by the emitted infrared radiation:

$$R_n = R_G(1-\alpha_t) + \epsilon_t\left(R_A - \sigma_{SB} {T_s}^4\right) \quad (6.89)$$

where σ_{SB} is the Stefan-Boltzmann constant.
The turbulent fluxes are calculated by means of the classical aerodynamic formulas. For the sensible heat flux:

$$H = \rho_a c_p C_H V_a (T_s - T_a) \quad (6.90)$$

where c_p is the specific heat; ρ_a, V_a, and T_a are respectively the air density, the wind speed, and the temperature at the lowest atmospheric level; and C_H, as discussed below, is the drag coefficient depending upon the thermal stability of the atmosphere. The explicit snow scheme sensible heat flux is calculated using the same formulation (but with T_{sn}). The water vapor flux E is the sum of the evaporation of liquid water from the soil surface (i.e., $E_{g\,l}$), from the vegetation (i.e., E_v), and sublimation from the snow and soil ice (i.e, E_s and $E_{g\,f}$):

$$LE = LE_{g\,l} + LE_v + L_i\,(E_s + E_{g\,f}) \quad (6.91)$$

$$E_{g\,l} = (1-veg)(1-p_{sng})\,(1-\delta_i)\;\rho_a C_H V_a\,(h_u q_{sat}(T_s) - q_a) \quad (6.92)$$

$$E_v = veg(1-p_{snv})\rho_a C_H V_a h_v\,(q_{sat}(T_s) - q_a) \quad (6.93)$$

$$E_s = p_{sn}\rho_a C_H V_a\,(q_{sat}(T_s) - q_a) \quad (6.94)$$

$$E_{g\,f} = (1-veg)\,(1-p_{sng})\;\delta_i\,\rho_a C_H V_a\,(h_{ui}\,q_{\rm sat}\,(T_s)\;-\;q_a) \quad (6.95)$$

where L and L_i are the specific heat of evaporation and sublimation, $q_{sat}(T_s)$ is the saturated specific humidity at the temperature T_s, and q_a is the atmospheric specific humidity at the lowest atmospheric level. The water vapor flux E from the explicit snow surface is expressed as

$$\begin{aligned} LE\left(T_{sn\,1}\right) &= LE_{sl} + L_i E_s && (6.96)\\ E_{sl} &= \delta_{sn}\,\rho_a C_{Hs} V_a \left(q_{sat}\left(T_{sn\,1}\right) - q_a\right) && (6.97)\\ E_s &= \left(1-\delta_{sn}\right)\,\rho_a C_{Hs} V_a \left(q_{sat}\left(T_{sn\,1}\right) - q_a\right) && (6.98)\\ \delta_{sn} &= w_{sl\,1}/w_{sl\,\max 1}\,; \qquad 0 \le \delta_{sn} \le 1 && (6.99) \end{aligned}$$

where evaporation of liquid water is zero when $T_{sn\,1} < T_0$. The transfer coefficient (C_{Hs}) is calculated over the snow covered surface using the same formulation as C_H.
The surface ice fraction is is used to partition the bare soil latent heat flux between evaporation and sublimation, and it is defined as

$$\delta_i = w_{g\,f}/\left(w_{g\,f} + w_g\right)\,; \qquad 0 \le \delta_i < 1\ . \tag{6.100}$$

The relative humidity h_u at the ground surface is related to the superficial soil moisture w_g following

$$\begin{aligned} h_u &= \frac{1}{2}\left[1 - cos\left(\frac{w_g}{{w_{fc}}^*}\pi\right)\right]\ ,\ \text{if } w_g < {w_{fc}}^* && (6.101)\\ h_u &= 1 \qquad\qquad ,\ \text{if } w_g \ge {w_{fc}}^* && (6.102) \end{aligned}$$

where the field capacity with respect to the liquid water is defined using the modified soil porosity so that ${w_{fc}}^* = w_{fc}\, w^*_{sat}/w_{sat}$. The humidity for the ice covered portion of the grid box is calculated in a similar fashion as

$$\begin{aligned} h_{ui} &= \frac{1}{2}\left[1 - cos\left(\frac{w_{g\,f}}{{w_{fc}}^{**}}\pi\right)\right]\ ,\ \text{if } w_{g\,f} < {w_{fc}}^{**} && (6.103)\\ h_{ui} &= 1 \qquad\qquad ,\ \text{if } w_{g\,f} \ge {w_{fc}}^{**} && (6.104) \end{aligned}$$

where ${w_{fc}}^{**} = w_{fc}(w_{sat} - w_g)/w_{sat}$. In case of dew flux when $q_{sat}(T_s) < q_a$, h_u is also set to 1 (see Mahfouf and Noilhan 1991 for details). When the flux E_v is positive, the Halstead coefficient h_v takes into account the direct evaporation E_r from the fraction δ of the foliage covered by intercepted water, as well as the transpiration E_{tr} of the remaining part of the leaves:

$$\begin{aligned} h_v &= (1-\delta)R_a/(R_a + R_s) + \delta && (6.105)\\ E_r &= veg(1-p_{snv})\frac{\delta}{R_a}\left(q_{sat}(T_s) - q_a\right) && (6.106)\\ E_{tr} &= veg(1-p_{snv})\frac{1-\delta}{R_a + R_s}\left(q_{sat}(T_s) - q_a\right) && (6.107) \end{aligned}$$

When E_v is negative, the dew flux is supposed to occur at the potential rate, and h_v is taken equal to 1.
Following Deardorff (1978), δ is a power function of the moisture content of the interception reservoir:

$$\delta = \left(W_r/W_{rmax}\right)^{2/3} \tag{6.108}$$

The aerodynamic resistance is $R_a = (C_H V_a)^{-1}$. The surface resistance, R_s, depends upon both atmospheric factors and available water in the soil; it is given by:

$$R_s = \frac{R_{smin}}{F_1 F_2 F_3 F_4 LAI} \tag{6.109}$$

with the limiting factors F_1, F_2, F_3, and F_4:

$$F_1 = \frac{f + R_{smin}/R_{smax}}{1+f} \tag{6.110}$$

$$F_2 = \frac{w_2 - w_{wilt}}{w_{fc} - w_{wilt}} \quad and\, 0 \leq F_2 \leq 1 \tag{6.111}$$

$$F_3 = 1 - \gamma\,(q_{sat}(T_s) - q_a) \tag{6.112}$$

$$F_4 = 1 - 1.6 \times 10^{-3}(T_a - 298.15)^2 \tag{6.113}$$

where the dimensionless term f represents the incoming photosynthetically active radiation on the foliage, normalized by a species-dependent threshold value:

$$f = 0.55 \frac{R_G}{R_{Gl}} \frac{2}{LAI} \tag{6.114}$$

Moreover, γ is a species-dependent parameter (see Jacquemin and Noilhan 1990) and R_{smax} is arbitrarily set to $5000\ sm^{-1}$.
The surface fluxes of heat, moisture, and momentum can be expressed as

$$(\overline{w'\theta'})_s = \frac{H}{\rho_a c_p T_a/\theta_a} \tag{6.115}$$

$$(\overline{w'r'_v})_s = \frac{E}{\rho_a(1-q_a)} \tag{6.116}$$

$$|\overline{w'V'}|_s = C_D|V_a|^2 = u_*^2 \tag{6.117}$$

where r_v is the water vapor mixing ratio, w is the vertical motion, θ_a is the potential temperature at the lowest atmospheric level. The primes and overbars denote perturbation and average quantities. For the drag coefficients C_H and C_D, the formulation of Louis (1979) was modified in order to consider different roughness length values for heat z_0 and momentum z_{0h} (Mascart et al. 1995):

$$C_D = C_{DN} F_m\ ;\ C_H = C_{DN} F_h \tag{6.118}$$

with

$$C_{DN} = \frac{k^2}{[ln(z/z_0)]^2} \tag{6.119}$$

$$\tag{6.120}$$

where k is the Von Karmann constant. Also

$$F_m = 1 - \frac{10Ri}{1 + C_m\sqrt{|Ri|}} \quad if\ Ri \leq 0 \tag{6.121}$$

$$F_m = \frac{1}{1 + \frac{10Ri}{\sqrt{1+5Ri}}} \quad if\ Ri > 0 \tag{6.122}$$

and

$$F_h = \left[1 - \frac{15Ri}{1 + C_h\sqrt{|Ri|}}\right] \times \left[\frac{ln(z/z_0)}{ln(z/z_{0h})}\right] \qquad if\ Ri \leq 0 \tag{6.123}$$

$$F_h = \frac{1}{1 + 15Ri\sqrt{1 + 5Ri}} \times \left[\frac{ln(z/z_0)}{ln(z/z_{0h})}\right] \qquad if\ Ri > 0 \tag{6.124}$$

where Ri is the gradient Richardson number. The coefficients C_m and C_h of the unstable case are given by

$$C_m = 10{C_m}^* C_{DN}(z/z_0)^{p_m} \tag{6.125}$$

$$C_h = 15{C_h}^* C_{DN}(z/z_{0h})^{p_h} \times \left[\frac{ln(z/z_0)}{ln(z/z_{0h})}\right] \tag{6.126}$$

where C_m^*, C_h^*, p_m, and p_h are functions of the ratio $\mu = ln(z_0/z_{0h})$ only:

$$C_h^* = 3.2165 + 4.3431 \times \mu + 0.5360 \times \mu^2 - 0.0781 \times \mu^3 \tag{6.127}$$

$$C_m^* = 6.8741 + 2.6933 \times \mu - 0.3601 \times \mu^2 + 0.0154 \times \mu^3 \tag{6.128}$$

$$p_h = 0.5802 - 0.1571 \times \mu + 0.0327 \times \mu^2 - 0.0026 \times \mu^3 \tag{6.129}$$

$$p_m = 0.5233 - 0.0815 \times \mu + 0.0135 \times \mu^2 - 0.0010 \times \mu^3 \tag{6.130}$$

6.4.7 Summary of Useful Parameters

The parameters have been chosen in order to characterize the main physical processes, while attempting to reduce the number of independant variables. They can be divided into two categories: primary parameters needing to be specified by spatial distribution, and secondary parameters which values can be associated with those of the primary parameters.

In the present state of the method, the primary parameters describe the nature of the land surface and its vegetation coverage by means of only four numerical indices: the percentage of sand and clay in the soil, the dominant vegetation type, and the land-sea mask.

The secondary parameters associated with the soil type are evaluated from the sand and clay composition of the soil, according to the continuous formulation discussed in Giordani (1993) and Noilhan and Lacarrère (1995) (see Appendix). These parameters are:

- the saturated volumetric moisture content w_{sat};
- the wilting point volumetric water content w_{wilt};
- the field capacity volumetric water content w_{fc};
- the slope b of the retention curve;
- the soil thermal coefficient at saturation C_{Gsat};
- the value of C_1 at saturation (i.e., C_{1sat});
- the reference value of C_2 for $w_2 = 0.5w_{sat}$ (i.e., C_{2ref});

- the drainage coefficient C_3 ;
- the diffusion coefficients $C_{4\,ref}$ and C_{4b} ;
- and the coefficients a, p for the w_{geq} formulation.

On the other hand, the parameters associated with the vegetation can either be derived from the dominant vegetation type, or be specified from existing classification or observations. They are

- the fraction of vegetation veg;
- the depth of the soil column d_2 (or the root zone depth);
- the depth of the soil column d_3 (if third soil layer option in use);
- the minimum surface resistance R_{smin};
- the leaf area index LAI;
- the heat capacity C_v of the vegetation;
- the R_{Gl} and γ coefficients found in the formulation of the surface resistance R_s;
- and the roughness length for momentum z_0 and for heat z_{0h}.

Other necessary parameters are

- the albedo α
- the emissivity ϵ.
- and characteristic time scale for phase changes (currently constant) τ_i.

6.4.8 Apendix A: Continuous formulation of the soil secondary parameters

Following Giordani (1993), Noilhan and Lacarrère (1995), the sand and clay composition (i.e., $SAND$ and $CLAY$) are expressed in percentage.

The saturated volumetric water content (m^3m^{-3}):

$$w_{sat} = (-1.08SAND + 494.305) \times 10^{-3} \tag{6.131}$$

The wilting point volumetric water content (m^3m^{-3}):

$$w_{wilt} = 37.1342 \times 10^{-3}(CLAY)^{0.5} \tag{6.132}$$

The field capacity volumetric water content (m^3m^{-3}):

$$w_{fc} = 89.0467 \times 10^{-3}(CLAY)^{0.3496} \tag{6.133}$$

The slope of the retention curve:

$$b = 0.137CLAY + 3.501 \tag{6.134}$$

The soil thermal coefficient at saturation (Km^2J^{-1}):

$$C_{Gsat} = -1.557 \times 10^{-2} SAND - 1.441 \times 10^{-2} CLAY + 4.7021 \tag{6.135}$$

The value of C_1 at saturation:

$$C_{1sat} = (5.58CLAY + 84.88) \times 10^{-2} \tag{6.136}$$

The value of C_2 for $w_2 = 0.5 w_{sat}$:

$$C_{2ref} = 13.815 CLAY^{-0.954} \tag{6.137}$$

The coefficient C_3:

$$C_3 = 5.327 CLAY^{-1.043} \tag{6.138}$$

The coefficient C_{4b}:

$$C_{4b} = 5.14 \, + \, 0.115 \, CLAY \tag{6.139}$$

The coefficient $C_{4\,ref}$:

$$C_{4\,ref} \;\; = \;\; \frac{2(d_3 - d_2)}{(d_2 \, {d_3}^2)} {\log_{10}}^{-1} \left[\beta_0 + \sum_{j=1}^{3} \left(\beta_j \, SAND^j \, + \, \alpha_j \, CLAY^{\,j} \right) \right] \tag{6.140}$$

where the β_j $(j = 0, 3)$ coefficients are 4.42×10^{-0}, 4.88×10^{-3}, 5.93×10^{-4} and -6.09×10^{-6}. The α_j $(j = 1, 3)$ coefficients are defined as -2.57×10^{-1}, 8.86×10^{-3} and -8.13×10^{-5}.
The coefficients for the w_{geq} formulation:

$$a \;\; = \;\; 732.42 \times 10^{-3} CLAY^{-0.539} \tag{6.141}$$

$$p \;\; = \;\; 0.134 CLAY + 3.4 \tag{6.142}$$

6.4.9 Appendix B: Gaussian formulation for the C_1 coefficient

Following Giordani (1993) and Braud et al. (1993), for dry soils (i.e., $w_g < W_{wilt}$), the C_1 coefficient in Eq. (13) is approximated by the Gaussian distribution:

$$C_1(w) = C_{1max} exp \left[-\frac{(w_g - w_{max})^2}{2\sigma^2} \right] \tag{6.143}$$

In this expression,

$$C_{1max} \;\; = \;\; (1.19 w_{wilt} - 5.09) \times 10^{-2} T_s + (-1.464 w_{wilt} + 17.86) \tag{6.144}$$

$$w_{max} \;\; = \;\; \eta w_{wilt} \tag{6.145}$$

with

$$\eta = (-1.815 \times 10^{-2} T_s + 6.41) w_{wilt} + (6.5 \times 10^{-3} T_s - 1.4) \tag{6.146}$$

and

$$\sigma^2 = -\frac{W_{max}^2}{2ln \left(\frac{0.01}{C_{1max}} \right)} \tag{6.147}$$

6.5 References

Anderson, E. A., 1976: A point energy and mass balance model of a snow cover. *NOAA Tech. Rep. NWS 19*, 150 pp. U.S. Dept. of Commer., Washington, D.C.

Bhumralkar, C.M., 1975: Numerical experiment on the computation of ground surface temperature in an atmospheric general circulation model. *J. Appl. Meteor.*, **14**, 1246-1258.

Blackadar, A.K., 1976: Modeling the nocturnal boundary layer. *Proc. Third Symp. on Atmospheric Turbulence, Diffusion and Air Quality* , Boston, Amer. Meteor. Soc., 46-49.

Boone, A., J.-C. Calvet and J. Noilhan, 1999: Inclusion of a third soil layer in a land-surface scheme using the force-restore method, *J. Appl. Meteor.*, **38**, 1611-1630.

Boone, A., V. Masson, T. Meyers, and J. Noilhan, 2000: The influence of the inclusion of soil freezing on simulations by a soil-atmosphere-transfer scheme. *J. Appl. Meteor.*, **39**, 1544-1569.

Braud, I., J. Noilhan, P. Bessemoulin, P. Mascart, R. Haverkamp, and M. Vauclin, 1993: Bare-ground surface heat and water exchanges under dry conditions: Observations and parameterization. *Bound.-Layer Meteror.*, **66**, 173-200.

Chin, H.-N. S., M.J. Leach, G.A. Sugiyama, J.M. Leone, H. Walker, J.S. Nasstrom, and M.J. Brown, 2005: Evaluation of an Urban Canopy Parameterization in a Mesoscale Model Using VTMX and URBAN 2000 Data. *Mon. Weather Rev.*, **133**, 2043–2068.

Deardorff, J.W., 1978: Efficient prediction of ground surface temperature and moisture with inclusion of a layer of vegetation. *J. Geophys. Res.*, **20**, 1889-1903.

Deardorff, J.W., 1977: A parameterization of ground surface moisture content for use in atmospheric prediction models. *J. Appl. Meteor.*, **16**, 1182-1185.

Dickinson, R.E., 1984: Modeling evapotranspiration for three dimensional global climate models. *Climate Processes and Climate Sensitivity. Geophys. Monogr.*, **29**, 58-72.

Douville, H., 1994: Développement et validation locale d'une nouvelle paramétrisation du manteau neigeux. Note 36 GMME/Météo-France.

Douville, H., J.-F. Royer, and J.-F. Mahfouf, 1995: A new snow parameterization for the French community climate model. Part I: Validation in stand-alone experiments. *Climate Dyn.*, **12**, 21-35.

Giard, D., and E. Bazile, 1999: Implementation of a new assimilation scheme for soil and surface variables in a global NWP model. *Mon. Wea. Rev.*, **128**, 997-1015.

Giordani, H., 1993: Expériences de validation unidimensionnelles du schéma de surface NP89 aux normes Arpège sur trois sites de la campagne EFEDA 91. Note de travail 24 GMME/Météo-France.

Hamdi, R., and V. Masson, 2008: Inclusion of a Drag Approach in the Town Energy Balance (TEB) Scheme: Offline 1D Evaluation in a Street Canyon. *J. Appl. Meteorol. Clim.*, **47**, 2627–2644.

Jacquemin, B., and J. Noilhan, 1990: Validation of a land surface parameterization using the HAPEX-MOBILHY data set. *Bound.-Layer Meteor.*, **52**, 93-134.

Johnsson, H., and L.-C. Lundin, 1991: Surface runoff and soil water percolation as affected by snow and soil frost. *J. Hydro.*, **122**, 141-158.

Lemonsu, A., V. Masson, L. Shashua-Bar, E. Erell, and D. Pearlmutter, 2012: Inclusion of vegetation in the Town Energy Balance model for modelling urban green areas. *Geosci. Model Dev.*, **5**, 1377–1393.

Loth, B., H.-F. Graf, and J. M. Oberhuber, 1993: Snow cover model for global climate simulations. *J. Geophys. Res.*, **98**, 10451-10464.

Louis, J.F., 1979: A parametric model of vertical eddy fluxes in the atmosphere. *Bound.-Layer Meteor.*, **17**, 187-202.

Lynch-Stieglitz, M., 1994: The development and validation of a simple snow model for the GISS GCM. *J. Clim.*, **7**, 1842-1855.

Mahfouf, J.-F., J. Noilhan, and P. Péris, 1994: Simulations du bilan hydrique avec ISBA: Application au cycle annuel dans le cadre de PILPS. Atelier de modélisation de l'atmosphère, CNRM/Météo-France, December 1994, Toulouse, France, 83-92.

Mahfouf, J.-F., and J. Noilhan, 1991: Comparative study of various formulations of evaporation from bare soil using in situ data. *J. Appl. Meteor.*, **9**, 1354-1365.

Martilli, A., A. Clappier, and M.W. Rotach, 2002: An Urban Surface Exchange Parameterisation for Mesoscale Models. *Bound.-Lay. Meteorol.*, **104**, 261–304.

Mascart, P., J. Noilhan, and H. Giordani, 1995: A modified parameterization of flux-profile relationships in the surface layer using different roughness length values for heat and momentum. *Bound.-Layer Meteor.*, **72**, 331-344.

Masson, 2000: A physically-based scheme for the urban energy budget in atmospheric models. *Bound. Layer. Meteor.*, **94**, 357-397.

Noilhan, J., and P. Lacarrère, 1995: GCM grid-scale evaporation from mesoscale modeling. *J. Climate*, **8**, 206-223.

Noilhan, J., and S. Planton, 1989: A simple parameterization of land surface processes for meteorological models. *Mon. Wea. Rev.*, **117**, 536-549.

Raupach, R.: Drag and drag partition on rough surfaces. *Bound.-Lay. Meteorol.*, **60**, 375–395.

Schoetter, R., Y.T. Kwok, C. de Munck, K.K.L. Lau, W.K. Wong, and V. Masson, 2020: Multilayer coupling between SURFEX-TEB-v9.0 and Meso-NH-v5.3 for modelling the urban climate of high-rise cities. *Geosci. Model Dev.*, **13**, 5609–5643.

Sun, S., J. Jin, and Y. Xue, 1999: A simple snow-atmosphere-soil transfer (SAST) model. *J. Geophys. Res.*, **104**, 19587-19579.

Verseghy, D., 1991: CLASS - A Canadian land surface scheme for GCMs. I: Soil model. *Int. J. Climatol.*, **11**, 111-133.